5-2013

MAGNETIC MANIPULATION OF PARTICLES AND CELLS IN FERROFLUID FLOW THROUGH STRAIGHT MICROCHANNELS USING TWO MAGNETS

Jian Zeng
Clemson University, jzeng@g.clemson.edu

MAGNETIC MANIPULATION OF PARTICLES AND CELLS IN FERROFLUID FLOW THROUGH STRAIGHT MICROCHANNELS USING TWO MAGNETS

A Thesis
Presented to
the Graduate School of
Clemson University

In Partial Fulfillment
of the Requirements for the Degree
Master of Science
Mechanical Engineering

---

by
Jian Zeng
May 2013

Accepted by:
Dr. Xiangchun Xuan, Committee Chair
Dr. Jay Ochterbeck
Dr. Chenning Tong

ABSTRACT

Microfluidic devices have been increasingly used in the past two decades for particle and cell manipulations in many chemical and biomedical applications. A variety of force fields have been demonstrated to control particle and cell transport in these devices including electric, magnetic, acoustic, and optical forces etc. Among these particle handling techniques, the magnetic approach provides clear advantages over others such as low cost, noninvasive, and free of fluid heating issues. However, the current knowledge of magnetic control of particle transport is still very limited, especially lacking is the handling of diamagnetic particle. This thesis is focused on the magnetic manipulation of diamagnetic particles and cells in ferrofluid flow through the use of a pair of permanent magnets. By varying the configuration of the two magnets, diverse operations of particles and cells is implemented in a straight microchannel that can potentially be integrated into lab-on-a-chip devices for various applications.

First, an approach for embedding two, symmetrically positioned, repulsive permanent magnets about a straight rectangular microchannel in a PDMS-based microfluidic device is developed for particle focusing. Focusing particles and cells into a tight stream is often required in order for continuous detection, counting, and sorting. The closest distance between the magnets is limited only by the size of the magnets involved in the fabrication process. The device is used to implement and investigate the three-dimensional magnetic focusing of polystyrene particles in ferrofluid microflow with both top-view and side-view visualizations. The effects of flow speed and particle size on the

particle focusing effectiveness are studied. This device is also applied to magnetically focus yeast cells in ferrofluid, which proves to be biocompatible as verified by cell viability test. In addition, an analytical model is developed and found to be able to predict the experimentally observed particle and cell focusing behaviors with reasonable agreement.

Next, a simple magnetic technique to concentrate polystyrene particles and live yeast cells in ferrofluid flow through a straight rectangular microchannel is developed. Concentrating particles to a detectable level is often necessary in many applications. The magnetic field gradient is created by two attracting permanent magnets that are placed on the top and bottom of the planar microfluidic device and held in position by their natural attractive force. The effects of flow speed and magnet-magnet distance are studied and the device was applied for use for concentrating live yeast cells. The magnet-magnet distance is mainly controlled by the thickness of the device substrate and can be made small, providing a locally strengthened magnetic field as well as allowing for the use of dilute ferrofluid in the developed magnetic concentration technique. This advantage not only enables a magnetic/fluorescent label-free handling of diamagnetic particles but also renders such handling biocompatible.

Lastly, a device is presented for a size-based continuous separation of particles through a straight rectangular microchannel. Particle separation is critical in many applications involving the sorting of cells. A first magnet is used for focusing the particle mixture into a single stream due to its relative close positioning with respect to the

channel, thus creating a greater magnetic field magnitude. Then, a following magnet is used to displace the aligned particles to dissimilar flow paths by placing it farther away compared the first magnet, which provides a weaker magnetic field, therefore more sensitive towards the deflection of particles based on their size. The effects of both flow speed and separator magnet position are examined. The experimental data are found to fit well with analytical model predictions. This is followed by a study replacing the particles which are closely sized to that of live yeast cells and observe the separation of the cells from larger particles. Afterwards, a test for biocompatibility is confirmed.

ACKNOWLEDGEMENTS

I would like to thank Dr. Xiangchun Xuan for giving me the opportunity to work in his laboratory as well as mentoring me throughout my graduate studies. His continuing academic support, guidance in project management, and effort in providing me with graduate funding are much appreciated.

Thank you to Dr. Jay Ochterbeck and Dr. ILenia Battiato for allowing me to work with you. Given the opportunity to be your grading assistant have enriched my Clemson graduate school experience within the Mechanical Engineering department. My enrollment within this department would not have been possible without this program's steady funding.

I wish to also thank Dr. Tzuen-Rong Tzeng and Pallavi Vedantam from Clemson University's Department of Biological Sciences for providing biological sample materials, of which was necessary in the completion of the projects involved in my graduate studies.

To my colleagues Junjie Zhu, Litao Liang, Saurin Patel, Chen Chen, and Yanxiang Deng, thank you for your help in contributing to my laboratory experience, paper writing, presentation run throughs, computer simulation support, and my overall graduate studies experience.

I would like to express my deepest gratitude towards my immediate and extended family for their enduring love and encouragement throughout my life.

TABLE OF CONTENTS

Page

Table of Contents (Continued)

Page

Table of Contents (Continued)

Page

LIST OF FIGURES

List of Figures (Continued)

Figure Page

List of Figures (Continued)

Figure Page

List of Figures (Continued)

Figure Page

List of Figures (Continued)

Figure Page

List of Figures (Continued)

Figure Page

NOMENCLATURE

$\mathbf{F}_{\mathrm{m}}$	particle experienced magnetic force
μ_0	permeability of free space
V_p	particle volume
$\mathbf{M}_{\mathrm{p}}$	particle magnetization
$\mathbf{M}_{\mathrm{f}}$	fluid magnetization
$\mathbf{H}$	magnetic field
$\mathbf{U}_m$	magnetophoretic induced velocity
$\mathbf{U}_p$	particle velocity
$\mathbf{U}_f$	fluid velocity
ϕ	volume fraction of magnetic nanoparticles
a	radius of diamagnetic particles
η	ferrofluid viscosity
f_D	drag coefficient
M_d	saturation moment of magnetic nanoparticles
$L(\alpha)$	Langevin function
H	magnitude of magnetic field

d	average diameter of magnetic nanoparticles
k_B	Boltzman constant
T	ferrofluid temperature
$\mathbf{r}_0$	initial position of particle
$\mathbf{r}_p$	particle position
t	time coordinate

CHAPTER 1

INTRODUCTION

1.1 Aims and Motivation

The field of microfluidics has seen tremendous growth in research within the past few decades. Beginning with the developments of micro-electromechanical systems (MEMS), the idea of miniaturization regarding machines and devices became a widely popular field of inquiry. As microfluidics is the study of fluid behavior at the micro-scale, conventional systems dealing with fluid processes see incredible advantages when downscaled towards the micro/nano domain due to the prospect of portability, cost effectiveness, quicker analysis, control precision, high throughput, and overall versatility. Most notably, microfluidics has played a crucial role in the development of inkjet print heads, Lab-on-a-Chip (LOC) devices, DNA microarrays, and micro-fluid/thermal technologies [1-8].

Within the scope of particle handling for both synthetic and biological materials, LOCs have been shown to be very effective. For the most part, particle manipulation consists of pumping a sample volume of solution with said particles in suspension from one area of the device to another through various influence of microfluidic transport. While in transport, the particles can be focused from an initial mixture to a single file stream for such applications as cytometry [9-11]. Also, the trapping of particles can occur by a directly applied force in opposition with respect to its flow (particle motion) and subsequently allow for a localized concentration [12,13]. Particle concentration plays

vital roles in bio-applications involving detection. Moreover, particles can be separated and sorted from a mixture based on a number of particle properties such as size, magnetization, and electrical conductivity [14,15].

A number of force field types can induce particle motion. Current popular methods include electric [16], magnetic [17], acoustic [18], and optical [19]. Among these, the magnetic approach provides many advantages comparatively, which is briefly reviewed in the following section. The magnetic approach can be separated into two distinct methods, positive and negative magnetophoresis, of which little work has been reported regarding the latter. Diamagnetic particles suspended within a magnetized medium experience a deflection force when introduced to a non-uniform magnetic field. As the difference in magnetization of diamagnetic materials and dilute ferrofluid is capable for micro-particle manipulation, permanent magnets provide ample field strength to handle cells with biocompatibility. It is in this interest that the following thesis is dedicated to the fundamental study of micro-particle and cell manipulation in a rectangular cross sectioned microchannel utilizing the negative magnetophoresis phenomenon. The next section will provide more information on the general aspects of particle manipulation in microfluidic devices and why they can be improved through the use of the magnetic approach.

1.2 Particle Manipulation Methods in Microfluidic Devices Background

Dielectrophoresis (DEP) has been a widely used technique for handling cell manipulation by utilizing microchannel geometries as electrokinetic motion can be enhanced at locations of non-uniform electric field gradients. As particle diameter is

directly proportional the DEP force, size-based separation can be taken advantage of [20]. Magnetophoresis, on the other hand, is the induced motion behavior of particles within the presence of a magnetic field gradient. Within the magnetic field, a magnetic force is experienced by a particle due to its proportionality to the particle's volume and therefore can be used to control particle action [21]. Acoustic waves can induce particle movements via its oscillatory propagation by adjusting frequency and wavelength. Acoustics have also been found to be capable of even more complex functions such as that of a microgripper that very accurately fetches individual particles within a channel [22]. Optical techniques can be used to directly influence a particle's behavior while in suspension using radiative light forces. Recently, the idea of optical tweezers have extended as far as to show direct self-assembly of particles at the nano-scale [23].

While all of the above mentioned means for particle manipulation prove successful and to each their own advantages, the magnetic approach is potentially the simplest and cheapest. Most notably, particle motion induced by a magnetic field is absent of fluid heating issues which is important to take into considering when handling biological materials such as living cells [24]. In the past, a magnetic approach to manipulation required the certain particle to be magnetically labeled which is invasive to a cell structure's integrity. This requirement is due to a biological cell's intrinsic nature of being diamagnetic. In an effort to avoid this intrusion, non-magnetic particle suspension in ferrofluids have gained attention as there are no magnetic tagging. The method of diamagnetic particle manipulation in ferrofluid microflows has been demonstrated in a number of recent studies [21,25-30].

Feasibility of diamagnetic particle focusing, concentration, and sorting are examined in this thesis via means of negative magnetophoresis using configurations of a pair of commercially available permanent magnets. The follow sections within this chapter will provide background information on the subject matter of magnetophoresis, more specifically negative magnetophoresis as it affords the mechanism for label free magnetic control of diamagnetic synthetic particles and biological cells. It will then close with the thesis structure pertaining to projects involved in the ensuing chapters.

1.3 Background on Particle Magnetophoresis

In recent times, the implementations of magnetophoresis for manipulating particles have shown prominence [17]. Magnetophoresis is the induced particle motion within the presence of a non-uniform magnetic field. Comparable to that of DEP, the mechanism of magnetophoresis can be positive or negative contingent on the magnetization of the particles relative to the medium in which it is suspended within [31]. Positive magnetophoresis describes the attractive motion of magnetic particles as it is pulled towards a magnetic field source (magnetic particles suspended in a nonmagnetic medium) while negative magnetophoresis depicts the behavior of non-magnetic particles as it is repelled away from a magnetic field source along its gradient (diamagnetic or nonmagnetic particle suspended in a magnetized medium) [24,32]. Figure 1 illustrates the two effects.

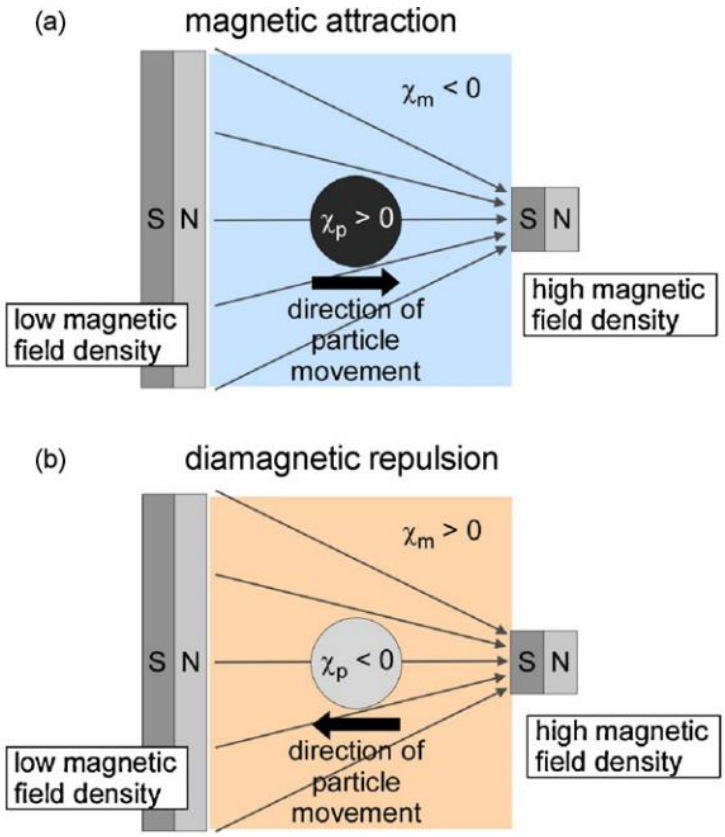

Figure 1: Illustration of positive (a) and negative (b) magnetophoretic phenomenon. (a) A particle that is more magnetized than its medium ($\mathbf{M}_f < \mathbf{M}_p$), will experience induced motion towards the magnetic source. (b) A particle that is less magnetized than its medium ($\mathbf{M}_p < \mathbf{M}_f$), will be repelled along the gradient of the magnetic field. Note that this figure shows particle and medium magnetic susceptibility rather than magnetization as their work focused on using uniform paramagnetic solution rather than ferrofluid, reprint from [33].

The magnetic force, $\mathbf{F}_m$, acting on the particle is defined as [34]:

$$\mathbf{F}_m = \mu_0 V_p \left[\left(\mathbf{M}_p - \mathbf{M}_f \right) \bullet \nabla \right] \mathbf{H} \tag{1}$$

Where μ_0 is the permeability of free space ($4\pi \times 10^{-7}$ H/m), V_p is the particle volume, $\mathbf{M}_p$ and $\mathbf{M}_f$ are the particle and fluid, respectively, and $\mathbf{H}$ is the magnetic field induced upon the particle. When $\mathbf{M}_f < \mathbf{M}_p$, the magnetic force yields a positive value corresponding to

positive magnetophoresis while $\mathbf{M}_f > \mathbf{M}_p$ produces a negative magnetic force value, offering negative magnetophoresis.

As mentioned previously, magnetic labeling of diamagnetic particles is required for manipulation under the influence of positive magnetophoresis. While on the other hand, negative magnetophoresis does not require it and is deemed advantageous as the majority of biological materials are intrinsically diamagnetic [26]. Commercially available and bio-compatible paramagnetic solutions or ferrofluids then can be used as the working medium for which these diamagnetic particles are suspended in.

This following works within this thesis will focus on the phenomenon of negative magnetophoresis of diamagnetic particles in ferrofluids as it has had less fundamental studies compared to that of positive magnetophoresis. However, a brief section on the study of positive magnetophoresis will be covered here to provide context on the recent developments in this topic.

1.3.1 Positive Magnetophoresis

The use of a magnetic field for directing magnetically tagged particles has had great success in the area of biomedical research. For example, drug delivery within the human body is a great concern for modern medicine. Magnetically tagged drugs can be given and transported once entering the body by means of an externally controlled magnetic field [35]. This method has shown to deliver drugs to certain areas of the circulatory system and proves a great advantage since there is no need for physically imposing surgery. Magnetic particles can also be used as solid supports for bioassays where magnetic particles can form plugs by inducing an external magnet field rather than

using physical obstructions. These plugs feature high surface to volume ratios and can be easily removed by detaching the magnet [36].

Other applications include magnetic separation where biological cells such as tumor can be sorted from red blood cells [37], hyperthermia treatment [38], and improving magnetic resonance imaging by contrast enhancement as well as a new invention of magnetic particle imaging [39]. Applications involving magnetic particles prove an invaluable tool in the field of microfluidics and biomedicine. These and additional reports regarding the uses of magnetic particles are reviewed by Pankhurst et al. [40,41], Pamme [17], Liu et al. [42], and Gijs et al. [24,43].

1.3.2 Negative Magnetophoresis

Works involving negative magnetophoresis of diamagnetic particles in paramagnetic solutions have been much less studied. Compared to ferrofluids, which are colloidal suspensions of magnetic nanoparticles in water or oil, paramagnetic solutions have a magnetic susceptibility several orders lower [44]. This causes a problem since its salt concentration must be increased significantly for particle stimulation, which in turn triggers issues in biocompatibility [10]. Ferrofluids, on the other hand, can be dilute and still allow for particle manipulation. However, many reports require particles and cells to be fluorescently stained as ferrofluids are opaque liquids. To avoid artificially staining biological cells as this may harm cell integrity, the magnetic field strength can be increased in combination with further ferrofluid dilution.

Dealing with diamagnetic particle handling in dilute ferrofluid, the magnetic field can be strengthened by either using more powerful magnets or by placing the magnet

closer to the particle flow. While utilizing more powerful magnets such as superconducting magnets is possible, it is not feasible for use on a LOC device, especially from the portability point of view due to complicated experimental setups. Taking this into consideration, it is more practical using cheap and commercially available permanent magnets by placing them as close to a microchannel flow as viable. This approach has been recently employed by Feinstein et al. [45] for self-assembly, Zhu et al. [30] for particle focusing, and Zhu et al. [29] for separation. The goal of this thesis is to provide detailed contributions towards this particular study of utilizing negative magnetophoresis for diamagnetic particle manipulation in ferrofluid filled microchannel flows constrained within a LOC device.

1.4 Thesis Arrangement

This thesis aims to provide demonstrations of using negative magnetophoresis for fundamental diamagnetic particle and cell handling in a microfluidic device. Making use of two permanent magnets, particles and cells will be focused, concentrated, and separated within a rectangular cross sectioned microchannel. To start, Chapter 2 will present an approach for embedding a pair of repulsive magnets and show visual evidence of a 3-D focusing. Next, Chapter 3 demonstrates a novel technique for magnetic trapping and concentration by utilizing the magnet's natural behavior. Then, Chapter 4 studies a size-based particle separation. Following the use of polystyrene particles, live yeast cells will be used in each device to show mechanistic compatibility. Within each of these works, the particular background on the area will be covered and, despite the fact that the experimental preparations, setups, and theory are similar to an extent, they will also be

discusses independently in their respective chapters to keep consistency and prevent the reader from frequently referencing prior chapters. Chapters 2 and 4 will also provide analytical solution supporting experimental findings. To conclude, Chapter 5 summarizes the key points of this thesis and looks at the prospects of future projects.

CHAPTER 2

FOCUSING

2.1 Background

Focusing particles and cells into a tight stream is often required in order to continuously detect, count, and sort them for chemical and biomedical applications [14,15,46]. A variety of particle focusing methods have been developed in microfluidic devices, which rely on either sheath fluids such as sheath flow focusing [47-52] or lateral forces such as sheathless focusing to manipulate the suspending fluid or particles for transverse particle movement [53-55]. The latter can be further classified as active and passive depending on if the force field is externally applied or internally induced [11]. The active particle focusing methods involve an optical [56], acoustic [57,58], electric [59], and dielectrophoretic [60,61] force while passive particle focusing methods exploit the fluid and/or channel structure-induced inertial [62,63], hydrodynamic [64,65], viscoelastic [66,67], and dielectrophoretic [68,69] effects.

Magnetic approach to particle manipulation can be enhanced if the diamagnetic particles are suspended magnetic solutions [70-75]. In this direction, this research group [75] has recently employed a similar design for focusing diamagnetic particles suspended in ferrofluid, where the particles are focused to a tight stream along the interface of the ferrofluid and sheath water in a T-shaped microchannel. In other studies, Pamme's group [10,33] examined the magnetic focusing of both polystyrene particles and mammalian cells in paramagnetic solutions, where a specialized mechanical setup was employed to

precisely align two facing magnets about a circular micro capillary. However, this method is unsuitable for integration into lab-on-a-chip devices with a planar structure. Additionally, Mao's group [30] conducted a combined experimental and theoretical study of the magnetic focusing of polystyrene particles in ferrofluid flow through an on-chip rectangular microchannel. In their case, the focused 5 μm particle stream was still about 100 μm wide at the lowest tested speed.

In this work a developed approach to embedding two repulsive permanent magnets into a PDMS-based microfluidic device is realized. The closest distance between the magnets is limited only by the size of the magnets involved in the fabrication process, which, as shown later, is twice smaller in our device than that achieved by Mao's group [30] and can be further reduced. This developed device is used to investigate the magnetic focusing of polystyrene particles in ferrofluid in both the horizontal and vertical planes of a straight microchannel with top-view and side-view visualizations. Due to the induced negative magnetophoresis, diamagnetic particles are deflected across the ferrofluid and focused to a narrow stream flowing near the bottom wall of the channel center plane. The same device is also applied to test the feasibility of magnetic focusing of live cells in ferrofluid. In addition, a theoretical model is developed to simulate the magnetic focusing of diamagnetic particles and cells in ferrofluid microflow.

2.2 Experiment

2.2.1 Device Fabrication

The microchannel was fabricated with polydimethylsiloxane (PDMS) by the method of standard soft lithography [22,75,77]. Details for the fabrication process can be

referred to in Appendix A. In order to embed two opposing Neodymium-Iron-Boron (NdFeB) permanent magnets (B222, 1/8" × 1/8" × 1/8", K&J Magnets, Inc.) into the PDMS layer, three top magnets (two B222 and one B224, 1/8" × 1/8" × 1/4") and three bottom magnets (B421, 1/4" × 1/8" × 1/16", K&J Magnets, Inc.) were used to fix the magnet positions. The three bottom holder magnets were placed below a petri dish, having the dish and glass slide between the embedded and holder magnets. The three top holder magnets were placed in direct contact with the embedded ones. A picture of thus arranged magnets is shown in Figure 2(a), where the north and south poles of the embedded magnets are labeled. The inset of Figure 2(a) illustrates how the magnetic poles of the embedded and holder magnets are configured to form a stable holding. The distance between the two embedded magnets is determined by the dimensions of both the holder and the embedded magnets. A right-angle prism (NT32-526, Edmund Optics Inc.) was placed 700 μm away from the microchannel and 5 mm downstream of the magnets for side-viewing. It was fixed onto the glass slide using sticky tape [see Figure 2(a)].

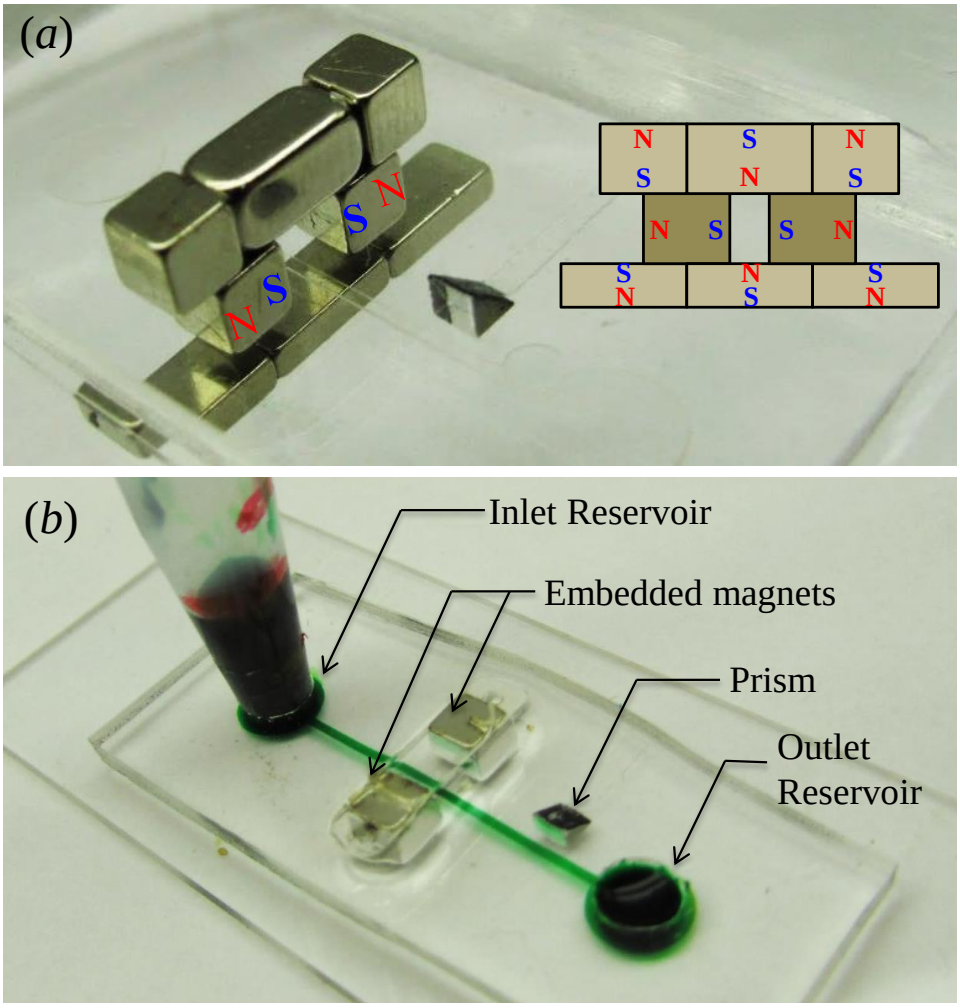

Figure 2: (a) Picture of the placed magnets and prism prior to the dispensing of liquid PDMS, where the inset shows how the magnetic poles of the embedded (middle row) and holder (top and bottom rows) magnets are configured to form a stable holding; (b) picture of the microfluidic device (the microchannel and reservoirs are filled with green food dye for clarity) used in the focusing experiment.

Once the prism and magnets were in place, liquid PDMS was dispensed to the dish and underwent the curing process. Following that, the holder magnets were removed and the reservoirs were created. Finally the PDMS slab was bonded to a glass slide. Further detail of this bonding process is described in Appendix A. Figure 2(b) shows a picture of the microfluidic device used in our experiments. The straight microchannel is 2 cm long and has a uniform cross-section of 600 μm (width) by 60 μm (depth). The two

embedded opposing magnets are symmetric about the microchannel with an edge-to-edge distance of 3.1 mm. This distance is roughly the size of the embedded magnet (1/8") and can be further reduced if smaller magnets (e.g., B111, 1/16" × 1/16" × 1/16", K&J Magnets, Inc.) are used.

2.2.2 Particle and Cell Solutions Preparation

A water-based ferrofluid, EMG 408, was obtained from Ferrotec (USA) Corp., which consists of 1.2% magnetic nanoparticles (10 nm diameter) by volume with a manufacturer identified saturation magnetization of 6.6 mT and viscosity of 2 mPa·s. Green fluorescent polystyrene particles of 5 μm diameter from Duke Scientific Corp. were originally packaged as 1% solids in water with size non-uniformity of 5% at most. By dilution using de-ionized water, the final solution used in our experiments was 0.25 × the original EMG 408 ferrofluid suspended with 5×10^6 particles/ml. For the experiment on a particle mixture, 1 μm green fluorescent polystyrene particles from Bangs Laboratory were directly suspended into the 5 μm particle solution to a concentration of 5×10^7 particles/ml.

Yeast cells (*Saccharomyces cerevisiae*) were cultured overnight in Sabouraud's dextrose broth in a shaker incubator at 30 °C, and were re-suspended in sterile PBS solution to a concentration of 5.73×10^8 cells/ml. In order to stain the live cells, 1 ul/ml of SYTO 9 was added to the yeast cell suspension. Prior to use, the stained yeast cells were washed with de-ionized water three times then re-suspended in 0.25× EMG 408 ferrofluid to a final concentration of around 5×10^6 cells/ml. The measured diameter of yeast cells is 5 μm on average. Tween 20 (Fisher Scientific) was added to both the particle and cell

suspensions at 0.1% by volume to minimize (or prevent) their aggregations and adhesions to microchannel walls.

2.2.3 Particle and Cell Manipulation and Visualization

The particle or cell suspension in ferrofluid was driven through the microchannel by adjusting the liquid height difference between the inlet and outlet reservoirs. A regular 1 ml pipette tip was inserted into the through hole in the PDMS slab serving as the inlet reservoir. Prior to experiment the solution in the outlet reservoir was vacated. The liquid height in the inlet reservoir was varied to achieve different flow speeds, which were first estimated through theoretical calculation and then verified via experimental tracking of individual particles [75,77]. The visualization of particle/cell motion was achieved using an inverted microscope (Nikon Eclipse TE2000U, Nikon Instruments, Lewisville, TX) equipped with a CCD camera (Nikon DS-Qi1Mc). Videos and images were recorded and processed using the Nikon imaging software (NIS-Elements AR 2.30).

2.3 Theory

2.3.1 Mechanism

Diamagnetic particles suspended in ferrofluid experience a magnetic force inside a non-uniform magnetic field, which deflects them away from the high field region at velocity, $\mathbf{U}_m$ [21],

$$\mathbf{U}_m = \frac{-\mu_0 \phi a^2}{9\eta f_D} \frac{M_d L(\alpha) \nabla \mathbf{H}^2}{H} \tag{2}$$

$$L(\alpha) = \coth(\alpha) - \frac{1}{\alpha} \quad \text{and} \quad \alpha = \frac{\pi \mu_0 M_d H d^3}{6 k_B T} \tag{3}$$

In the above, μ_0 is the permeability of free space, ϕ is the volume fraction of magnetic nanoparticles in the ferrofluid, a is the radius of diamagnetic particles, η is the ferrofluid viscosity, f_D is the drag coefficient to account for the particle-wall interactions [21,29,30,77,78], M_d is the saturation moment of magnetic nanoparticles, $L(\alpha)$ represents Langevin function [79], **H** is the magnetic field with a magnitude of H, d is the average diameter of magnetic nanoparticles, k_B is the Boltzmann constant, and T is the ferrofluid temperature. Note that the contribution of the magnetization of diamagnetic particles has been neglected in equation (2) because it is usually much smaller than that of the ferrofluid. For the magnetic field produced by a block magnet, Furlani's analytical model [80] can be applied if the ferrofluid is assumed to have a negligible effect on the magnetic field distribution. This has been proved reasonable in several recent studies [21,29,30,77,78].

The use of two opposing magnets of equal geometry and magnetization can create a non-uniform but symmetric magnetic field within the microchannel in the horizontal plane, where the minimum field occurs right along the channel centerline [10,30,33]. Therefore, diamagnetic particles are pushed horizontally away from the channel wall by magnetic force at velocity, $\mathbf{U}_m$, as they pass the magnet region along with the ferrofluid flow at velocity, $\mathbf{U}_f$. This is illustrated by the vector distribution of the magnetic force and the analysis of the particle velocity, $\mathbf{U}_p = \mathbf{U}_f + \mathbf{U}_m$, in Figure 3 (left plot, see also the contour of the magnetic force magnitude). Moreover, the two opposing magnets also generate magnetic field gradients in the vertical plane [21,75], inducing a magnetic force

on the particle toward the bottom wall of the microchannel; see the force vector and the induced magnetophoretic particle velocity in the right plot of Figure 3.

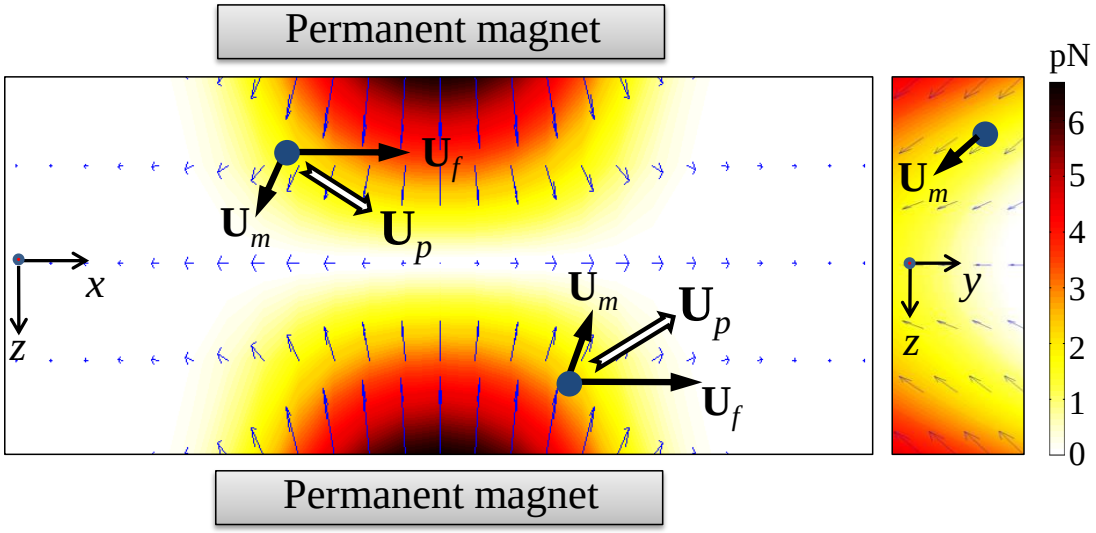

Figure 3: Velocity analysis of a diamagnetic particle suspended in a ferrofluid in the horizontal (left plot) and vertical (right plot) planes of the microchannel when subjected to the non-uniform magnetic field of two opposing magnets (not drawn to scale). The background color and arrows display the contour and the vector distribution of the magnetic force experienced by the particle.

The combined effect of the magnetically induced horizontal and vertical particle deflections is a focused particle stream near the bottom edge of the channel mid-plane. The effectiveness of such "three-dimensional" magnetic focusing can be simply measured by the ratio of the particle velocity perpendicular and parallel to the flow direction,

$$\text{Focusing} \propto \frac{U_{p,i}}{U_{p,x}} = \frac{U_{m,i}}{U_f + U_{m,x}} \approx \frac{U_{m,i}}{U_f} \quad (i = y, z) \tag{4}$$

where $U_{p,i}$ (i = x, y, z) denotes the particle speed in the directions of fluid flow (x), channel depth (y), and channel width (z), respectively, $U_{m,i}$ is the magnetophoretic particle speed in each of the three directions (refer to equation (2) for the

magnetophoretic velocity), and U_f is the ferrofluid flow speed. Note that the gravity induced particle sedimentation in the channel depth direction (y) is neglected in the last equation. This is justified by the close match of the mass densities of the ferrofluid (about 1.03 g/cm^3 for 0.25× EMG 408) and the particle (1.05 g/cm^3), which induces at most a sedimentation speed of 0.27 μm/s at most. Equation (4) along with equation (2) indicates that the diamagnetic particle focusing can be enhanced by increasing the particle size and ferrofluid concentration or decreasing the ferrofluid flow speed. Moreover, bringing closer the two opposing magnets can increase the magnetic field and gradients and hence enhance the particle focusing. In addition, using a longer magnet in the flow direction should also be beneficial as demonstrated by Zhu et al. [30].

2.3.2 Simulation

The analytical model that was developed in earlier works within this research group [21,77] was used to simulate the three-dimensional diamagnetic particle focusing in our experiments. The magnetic field distribution was obtained by superimposing the magnetic fields of the two opposing magnets, which was each computed from Furlani's analytical formula [80] and neglected here for conciseness. The diamagnetic particle was assumed massless and had the velocity, $\mathbf{U}_p = \mathbf{U}_f + \mathbf{U}_m$, as explained above (see Figure 3). The ferrofluid flow in the straight microchannel was assumed fully-developed and not affected by particle magnetophoresis. The flow velocity was assumed to follow the analytical formula for pressure-driven flow in a rectangular channel. The applied pressure drop across the channel was estimated from hydrostatic pressure by measuring the height difference of the liquid columns in the inlet and outlet reservoirs. The instantaneous

position of the particle center was computed by integrating $\mathbf{U}_p$ over time with respect to its initial position,

$$\mathbf{r}_p = \mathbf{r}_0 + \int_0^t \left[\mathbf{U}_f(t') + \mathbf{U}_m(t') \right] dt' \tag{5}$$

where $\mathbf{r}_0$ is the initial position of the particle, and t is the time coordinate. Simulation was performed in Matlab®. Further technical detail of the model implementation is described in the works of Liang et al. [21].

2.4 Results and Discussion

2.4.1 3D Focusing

The three-dimensional magnetic focusing of 5 μm polystyrene particles was studied in 0.25× EMG 408 ferrofluid at a mean flow speed of 0.4 mm/s (or equivalently a flow rate of 0.85 μl/min). This focusing in the horizontal plane of the microchannel (i.e., the channel width direction in top view) was visualized with videos recorded at two view windows along the channel length, where the first window is centered at the leading edge of the magnets relative to the fluid flow and the second window is about 5 mm downstream of the magnets' back edge; see the schematic (not to scale) on the top of Figure 4. Figure 4(a) presents the snapshot image (top), superimposed image (middle), and simulated particle trajectories (bottom) from the top view of each of these two locations. Note that the original images have been cropped and adjusted (in both contrast and brightness) for best view. The superimposed image was obtained by superimposing a sequence of more than 200 snapshot images over a 20 s timeframe. The horizontal focusing of 5 μm particles can be clearly seen in Figure 4(a1) as the particles enter the

magnet region with a nearly uniform distribution over the channel width and begin to get pinched towards the center of the microchannel by negative magnetophoresis.

Downstream from the magnets, the laminar flow allows for the magnetically deflected particles to remain in their positions relative to the width of the channel. As demonstrated in Figure 4(a2), particles move along the channel centerline in almost a single file (see the snapshot image in the top). The measured width of this focused particle stream (see in the superimposed image in the middle) is 35 μm, which seems to be much wider than the particle diameter (5 μm). This is because fluorescent particles look apparently larger than their real sizes in recorded images. These observed magnetic pinching and focusing behaviors of particles in the channel width direction are reasonably captured by the theoretical model (see middle and bottom rows in Figure 4(a)). However, the model seems to underpredict the particle focusing performance. The discrepancy between them may be due to the error in measuring the liquid height difference in the inlet and outlet reservoirs, which affects the ferrofluid flow speed and hence the particle focusing, see equation (4).

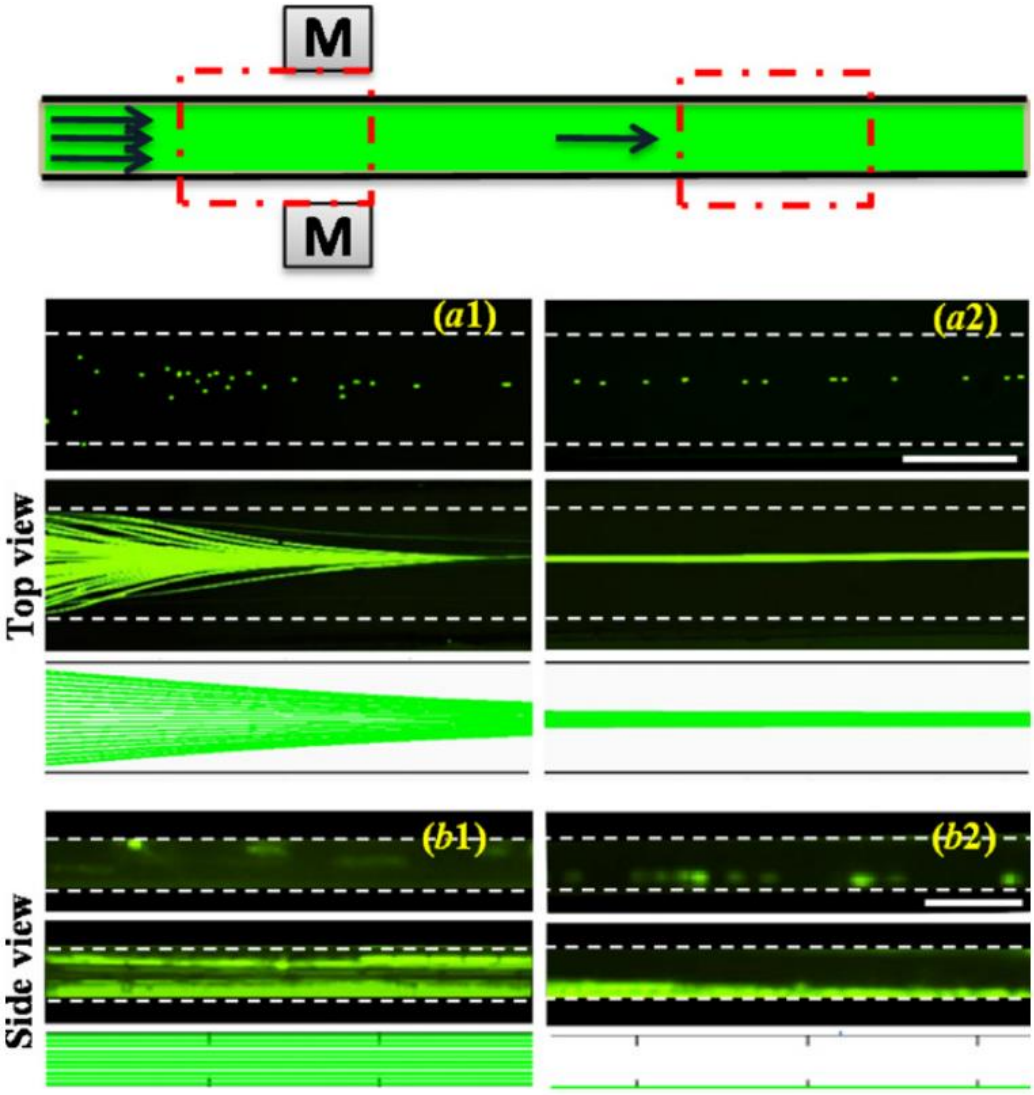

Figure 4: Experimental and theoretical results illustrate the three-dimensional magnetic focusing of 5 μm diamagnetic particles in 0.25× EMG ferrofluid through a straight microchannel at a mean flow speed of 0.4 mm/s: top views from the view window at the front edge of the magnets (*a*1) and the view window 5 mm downstream of the back edge of the magnets (*a*2); side views from the view window before the magnets (*b*1) and after the magnets (*b*2). The top, middle and bottom plots in each panel (i.e., (*a*1), (*a*2), (*b*1), and (*b*2)) show the experimentally obtained snapshot and superimposed images and the theoretically simulated particle trajectories, respectively. The flow direction is from left to right in all images. The scale bars in (*a*2) and (*b*2) represent 500 μm and 50 μm, respectively.

The magnetic focusing of 5 μm particles in the vertical plane of the microchannel (i.e., the channel depth direction in side view) was visualized through the use of the embedded prism and is demonstrated in Figure 4(b). The unfocused particle images in Figure 4(b1) were obtained when the ferrofluid flow direction in the microchannel was reversed. In other words, the prism shown in Figure 3 became actually located at the upstream of the magnets where particles were not magnetically deflected. In contrast, Figure 4(b2) shows the snapshot (top) and superimposed (middle) images of particles that have been vertically focused by the induced negative magnetophoresis in ferrofluid. As expected, the particles occupy the bottom surface of the channel [21,75] and migrate through the view window in a single file, which is also reasonably predicted by the theoretical model. Note that the particles in the side-view images look dim relative to those in the top-view images due to the optical interferences from the prism and its interfaces with PDMS.

2.4.2 Flow Speed Effects

The effect of ferrofluid flow speed on the magnetic focusing of 5 μm particles is presented in Figure 5. All parameters remain similar to those in Figure 4 during the test except that the flow speed is varied from 0.4 mm/s to 0.8 mm/s and 1.2 mm/s. Consistent with equation (4) that predicts a weaker focusing of particles suspended in a faster flow, the measured width of the focused particle stream (symbols with error bars in Figure 5) increases with the flow speed. This is because the faster the particles move, the less time they get exposed to the magnetic field gradient and hence experience less magnetic deflection. The inset images in Figure 5 illustrate the superimposed particle images at the

three tested flow speeds, which are all obtained at the view window 5 mm downstream of the back edge of the magnets. One can see in Figure 5 that the experimentally measured particle stream widths (symbols with error bars) agree closely with the theoretically predicted curve (solid line) within the experimental errors (10 μm for the error of measured stream width and 0.1 mm/s for the error of measured flow speed).

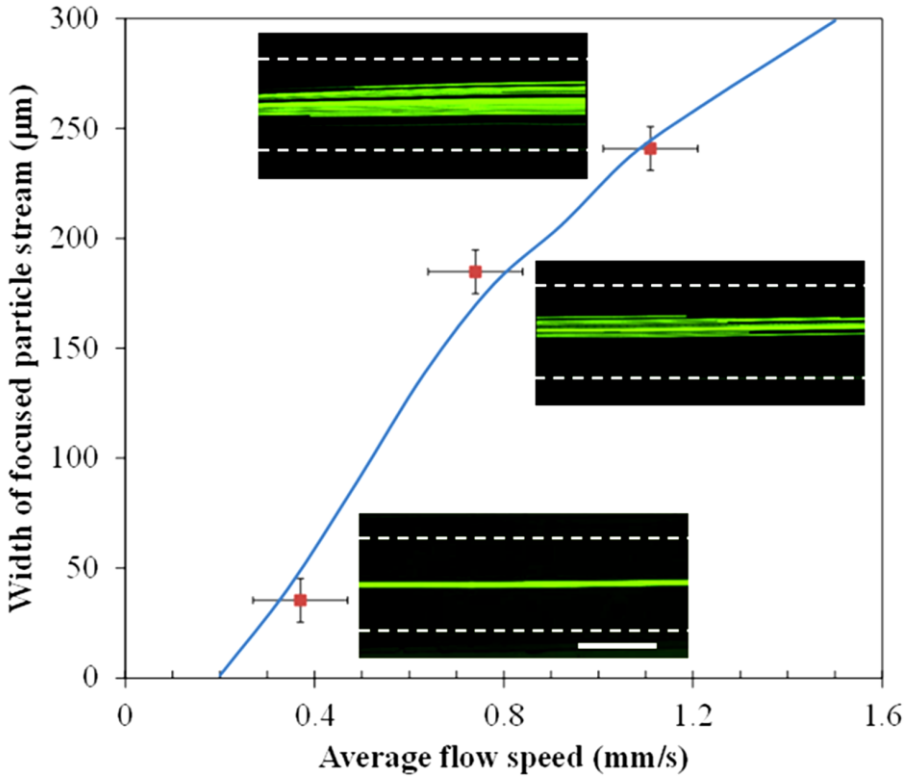

Figure 5: Ferrofluid flow speed effect on the magnetic focusing of 5 μm particles in the horizontal plane of the microchannel. The symbols with error bars represent the experimentally measured particle stream widths. The solid line is the theoretically predicted curve from the analytical model. The flow direction is from left to right in all the insets (superimposed particle images). The scale bar represents 500 μm.

2.4.3 Particle Mixture Focusing and Filtration

Figure 6 illustrates the magnetic focusing of 5 μm and 1 μm particle mixture in ferrofluid flow through the straight microchannel. The purpose of this experiment is two-fold: one is to examine the effect of the presence of other particles (of dissimilar

properties, here, of different sizes) on diamagnetic particle focusing, and the other is to demonstrate the particle size dependence of this focusing approach. The experimental conditions are the same as those in Figure 4. The layout of the images from the two view windows shown in Figure 6 is also identical to that in Figure 4. One can see in Figure 6(a) that as the particle mixture enters the magnetic region 5 μm particles undertake a much greater magnetic deflection than 1 μm ones. This is consistent with equation (2), which predicts a quadratic dependence of the induced magnetophoretic velocity on particle diameter. The result is that 5 μm particles are focused into a tight stream along the channel centerline while 1 μm particles are still distributed across the majority of the channel width as demonstrated in Figure 6(b). Moreover, the focusing of 5 μm particles appear similar to that shown in Figure 4, indicating an insignificant influence from the presence of 1 μm particles. These observed particle behaviors are properly captured by the theoretical model, where the green and red lines in Figure 6 (bottom row) represent the trajectories of 5 μm and 1μm particles, respectively. Such distinct motions of the two sizes of particles are envisioned to enable a continuous concentration and filtration of particles by size.

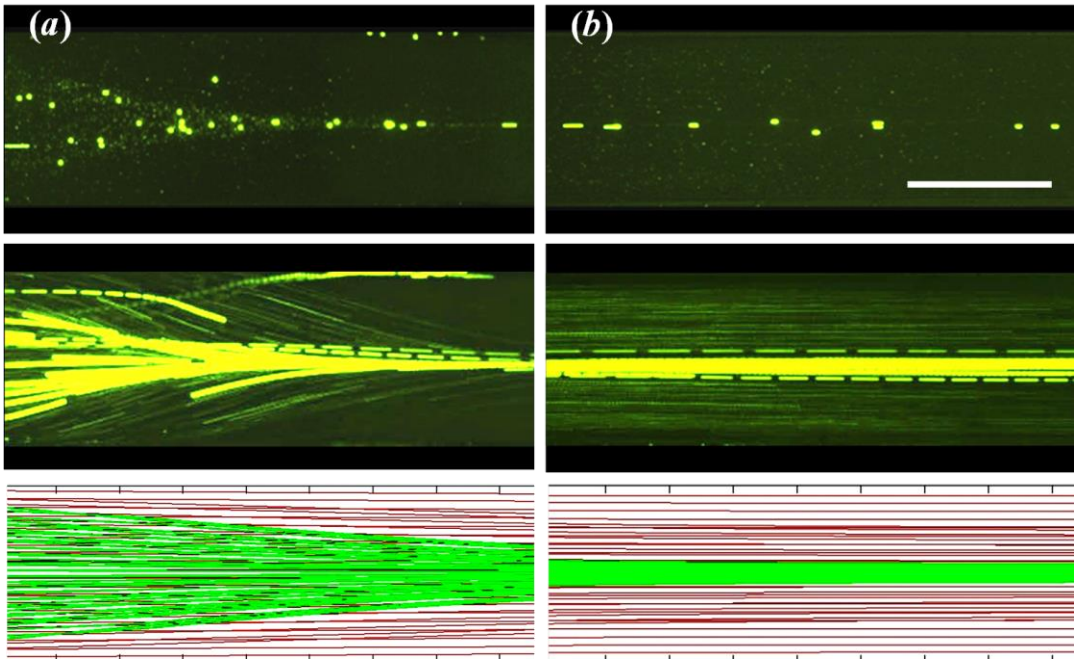

Figure 6: Experimental and theoretical results for the magnetic focusing of 5 μm and 1 μm particle mixture in ferrofluid microflow: top views from the view window at the front edge of the magnets (*a*) and the view window 5 mm downstream of the back edge of the magnets (*b*). The experimental conditions and the image layout are similar to Figure 4. The flow direction is from left to right. The scale bar represents 500 μm.

2.4.4 Live Yeast Cell Focusing

The magnetic focusing of live yeast cells in ferrofluid flow through the fabricated straight microchannel was also investigated. As the cells have an average diameter between 3 and 5 μm, similar experimental conditions to those for 5 μm polymer particles are used for this test. Figure 7 shows the top-view superimposed cell images obtained from the two view windows as noted in Figure 4. Snapshot images are not presented here due to the stained cells being far dimmer than fluorescent particles. The same pinching effect for the particles can be seen here for the cells at the front edge of the magnets (see the top image in Figure 7). Eventually cells move through the microchannel one by one and form into a focused stream of about 20 μm wide downstream of the magnets (see the

bottom image in Figure 7). The experimental images agree with the simulated cell trajectories that are presented in Figure 4(a) (bottom row).

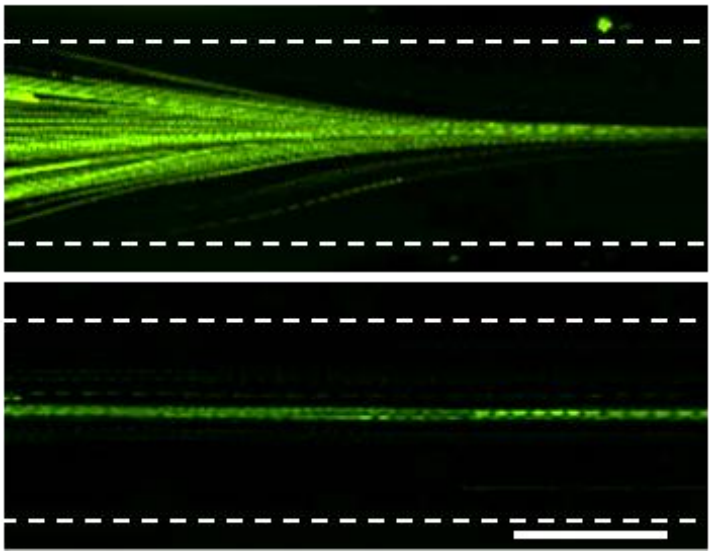

Figure 7: Experimentally obtained streak images show the magnetic focusing of yeast cells in ferrofluid at a mean flow speed of 0.4 mm/s. The images were obtained from the same view windows as explained in Figure 4. The simulated cell trajectories are similar to those presented in Figure 4 and not included here. The flow direction is from left to right in both images. The scale bar represents 500 µm.

A test for cell viability was performed using a spread plate technique, which enumerates and compares the total number of live yeast cells before and after magnetic focusing in the ferrofluid. In brief, a series of six 10-fold dilutions were carried out for the cell suspension collected from the outlet reservoir after focusing experiment. A 100 µl of the dilution was plated in triplicates on Potato Dextrose agar plates and incubated at 30 °C for 24 to 48 hours. Following that, the colonies were counted and the CFU/ml (Colony Forming Unit) was determined. The total number of cells counted was compared to that of the original cell suspension prior to being re-suspended to ferrofluid for magnetic focusing test. Only a 10% decrease in the cell count was found, indicating a good biocompatibility of the demonstrated magnetic focusing method in ferrofluid.

2.5 Summary

Here is an approach to embedding opposing permanent magnets about a straight planar microchannel with good accuracy. The distance between the two magnets is determined solely by the size of the magnets involved in the fabrication process, which is 3.1 mm or 1/8" for the tested microfluidic device. This device has been used to implement a three-dimensional magnetic focusing of 5 μm diamagnetic particles in ferrofluid at a mean flow speed of 0.4 mm/s. Such focusing results from the negative magnetophoretic particle motion and is demonstrated through visualization from both the top- and side-view of the microchannel. The effectiveness of this diamagnetic particle focusing in ferrofluid is enhanced when the flow speed is decreased and/or the particle size is increased. The latter has been demonstrated by differentially focusing a 5 μm and 1 μm particle mixture, indicating potential applications of the developed magnetic focuser to continuous concentration and filtration of particles by size. This device has also been tested for live yeast cells, which turns out to be biocompatible. Moreover, three-dimensional analytical model has been developed, which predicts with a good agreement the observed particle and cell focusing behaviors at various conditions.

CHAPTER 3

TRAPPING AND CONCENTRATION

3.1 Background

Concentrating particles to a detectable level is often necessary and critical in many applications such as environment monitoring, food safety, and water quality control [13,81]. In microfluidic devices, particles can be concentrated by means of contact or contactless methods [12]. Contact methods include the use of chemical, mechanical and physical processes for particle immobilization or blocking [82-87]. This type of methods allows for straightforward handling, but often suffers from irreversible particle adhesions. Contactless methods utilize an externally applied or internally induced force field, such as electric [84,88-95], optical [96,97], acoustic [98,99], and thermal [100] forces, to trap and enrich particles in suspensions. These methods allows for the concentration of particles while the force field is on and the release of the retained particles by simply turning the force field off. They, however, often require complex preparations, intricate microchannel designs, and expensive equipment.

Magnetic force has long been used to concentrate magnetic (or magnetically tagged) particles through positive magnetophoresis [17,24,42,43,70,76,101-103]. Like other contact methods, the trapped magnetic particles tend to form chains or clusters and cannot be completed removed from a surface even after the external magnetic field has been removed. Magnetic concentration of diamagnetic particles has been demonstrated in both paramagnetic solutions and ferrofluids using negative magnetophoresis. The

magnetic field gradient is created by the use of either repulsive [45,104,105] or attractive [33] magnets, where the particles are concentrated in between and outside the aligned magnets, respectively. The involving magnets need to be fixed using a special mechanical setup and have been implemented to work with micro capillaries only. In addition, diamagnetic particles can be concentrated in ferrofluids using patterned soft magnets or electromagnets [26,34,76,106,107], which, however, both require complicated device fabrications.

This work develops a simple magnetic technique to concentrate diamagnetic particles in ferrofluid flow through a straight rectangular microchannel using attracting permanent magnets. The two magnets are placed on the top and bottom of the planar microfluidic device and held in position by their natural attractive force, which eliminates the use of any special mechanical setup or specially designed magnets. Moreover, as the magnet-magnet distance can be made small by reducing the microchannel substrate thickness, a dilute ferrofluid is sufficient to implement a continuous magnetic concentration of 5 μm polystyrene particles and live yeast cells.

3.2 Experiment

The straight microchannel was fabricated using the standard soft lithography method and formed by bonding the PDMS slab with a glass cover slip (Fisher Scientific., 0.17-0.25 mm thick). It is straight and 2 cm long with a uniform width of 550 μm and a uniform depth of 60 μm. The detailed procedure for the microchannel fabrication is referred to Appendix A. Two attracting Neodymium-Iron-Boron (NdFeB) permanent magnets (B421, 1/4" × 1/8" × 1/16", K&J Magnetics Inc.) are placed above and below

the entire device, above the PDMS slab and underneath the cover slip, respectively. Their separating distance can be controlled by varying the thickness of the PDMS slab. Figure 8 shows a picture of the microfluidic device used in the particle/cell concentration experiments, where the inlet reservoir was formed by inserting a 1-ml pipette tip into the through hole in the PDMS slab. The particle or cell suspension was driven due to a pressure difference between the inlet and outlet via height difference.

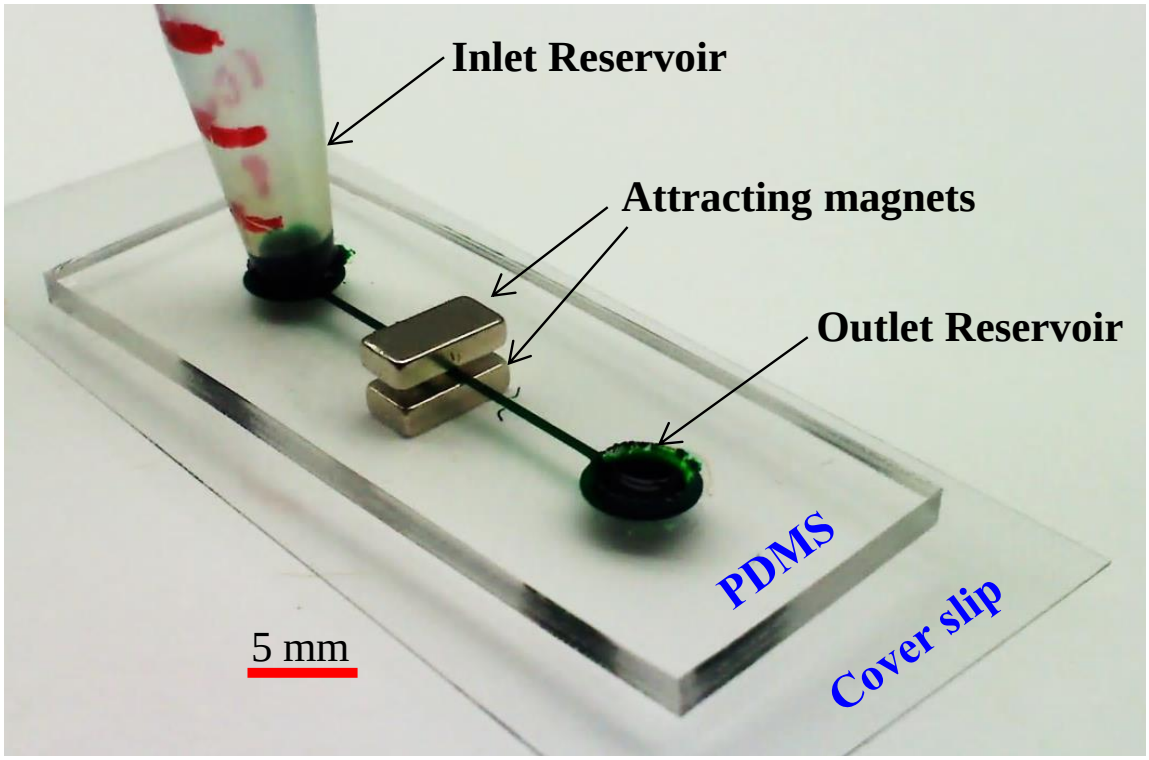

Figure 8: Picture of the microfluidic device (the microchannel and reservoirs are filled with green food dye for clarity) used in the trapping and concentration experiment. The two magnets are on top and bottom of the device and held by their natural attraction force.

The particle solution was made by suspending 5 μm polystyrene particles (Duke Scientific Corp.) in 0.05× EMG 408 ferrofluid (Ferrotec Corp.) to a concentration of 5×10^6 particles/ml. The dilute ferrofluid was prepared by mixing the original EMG 408

ferrofluid with pure water at a volume ratio of 1:19. Yeast cells (*Saccharomyces cerevisiae*) were cultured overnight in Sabouraud's dextrose broth in a shaker incubator at 30 °C, and were re-suspended in sterile phosphate buffered saline (PBS) solution to a concentration of 5.73×10^8 cells/ml. Prior to use, live yeast cells were washed with de-ionized water three times and re-suspended in 0.05× EMG 408 ferrofluid to a final concentration of around 5×10^6 cells/ml. The measured diameter of yeast cells is 3-5 μm on average. Tween 20 (Fisher Scientific) was added to both the particle and cell suspensions at 0.1% by volume to minimize their aggregations and adhesions to microchannel walls.

The particle or cell suspension in the diluted ferrofluid was introduced only to the inlet reservoir (see Figure 8). The liquid height in the inlet reservoir was varied to achieve different flow speeds. The outlet reservoir was emptied prior to experiment. To minimize the back-flow effects due to liquid build-up during the course of particle/cell concentration, the outlet reservoir was intentionally made large. Particle/cell motion was visualized using an inverted microscope (Nikon Eclipse TE2000U, Nikon Instruments, Lewisville, TX) under a bright-field illumination. Digital videos (at a time rate of around 12 frames per seconds) and images were recorded through a CCD camera (Nikon DS-Qi1Mc) and post-processed using the Nikon imaging software (NIS-Elements AR 2.30).

3.3 Theory and Mechanism

Diamagnetic particles undergo negative magnetophoresis in a ferrofluid when subjected to a non-uniform magnetic field. This motion, $\mathbf{U}_m$, points in the direction of decreasing magnetic field and is expressed as [21,75],

$$\mathbf{U}_m = \frac{-\mu_0 \phi a^2}{9\eta f_D} \frac{M_d L(\alpha) \nabla \mathbf{H}^2}{H} \tag{6}$$

$$L(\alpha) = \coth(\alpha) - \frac{1}{\alpha} \text{ and } \alpha = \frac{\pi \mu_0 M_d H d^3}{6 k_B T} \tag{7}$$

where μ_0 is the permeability of free space, ϕ is the volume fraction of magnetic nanoparticles in the ferrofluid, a is the radius of diamagnetic particles, η is the ferrofluid viscosity, f_D is the drag coefficient to account for the particle-wall interactions [21,29,30,73,77], M_d is the saturation moment of magnetic nanoparticles, $L(\alpha)$ represents Langevin function [108], **H** is the magnetic field with a magnitude of H, d is the average diameter of magnetic nanoparticles, k_B is the Boltzmann constant, and T is the ferrofluid temperature. Note that in equation (6) the contribution from the magnetization of diamagnetic particles has been neglected because it is nearly 4 orders of magnitude smaller than that of the ferrofluid used within this experiment. The magnetophoretic velocity, $\mathbf{U}_m$, increases for larger diamagnetic particles in a ferrofluid with a larger fraction of magnetic nanoparticles.

The use of two attracting magnets of equal geometry and magnetization in Figure 8 can confine the majority of the magnetic field lines in between the two polar surfaces. This in turn creates strong magnetic gradients within the microchannel at near the front and rear edges of the magnets as evidenced by the magnetic field contour (the darker color, the larger magnitude) in Figure 9. The magnetic field distribution was obtained by superimposing the magnetic fields of the two attracting magnets, which was each computed from Furlani's analytical formula [80]. Note that the ferrofluid effects on the

magnetic field are neglected in this analytical formula, which has been proved reasonable in recent studies [21,29,30,78]. As indicated by the arrow plots in Figure 9, the induced magnetophoretic velocity, $\mathbf{U}_m$, of diamagnetic particles is against the flow velocity of the suspending ferrofluid, $\mathbf{U}_f$. Therefore, particles will be stagnated at the locations that the two velocities are counterbalanced, leading to a continuous trapping and concentration of particles. Such a magnetic concentration works more effectively for larger diamagnetic particles in a ferrofluid with a higher volume fraction of magnetic nanoparticles. In addition, since $\mathbf{U}_m$ is nearly uniform across the microchannel while $\mathbf{U}_f$ has a parabolic profile (see the vector plots of these two opposing velocities in Figure 9), particles travelling along different flow paths should be stagnated at dissimilar locations. Specifically, particles travelling near the channel walls can be trapped further away from the magnet than those near the channel center. The interactions between the fluid and particles are hypothesized to cause a pair of counter-rotating circulations of the trapped particles as schematically illustrated in Figure 9.

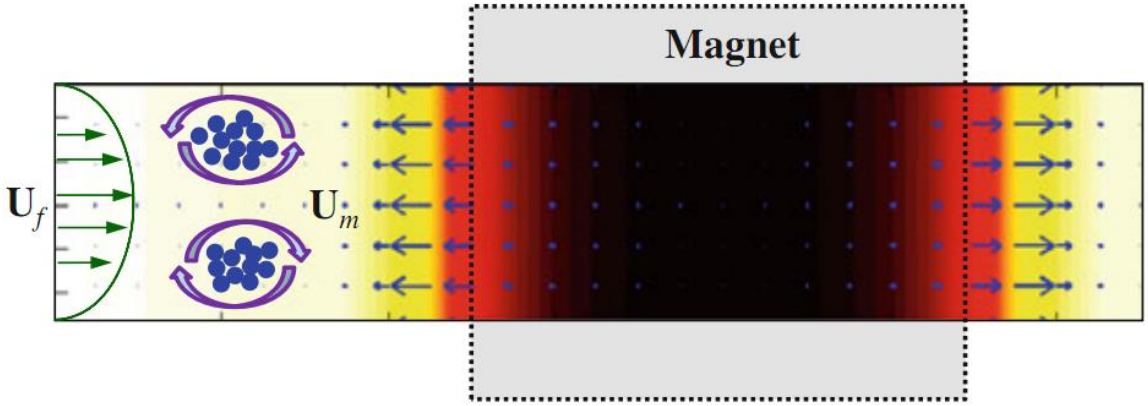

Figure 9: Illustration of the mechanism for magnetic concentration of diamagnetic particles in a pressure driven ferrofluid flow through a straight microchannel. The background color indicates the magnetic field contour (the darker, the larger magnitude). The thin arrows display the velocity vecotrs of ferrofluid flow, $\mathbf{U}_f$, particle magnetophoresis, $\mathbf{U}_m$. Particles are trapped in the locations where $\mathbf{U}_m$ can counterbalance $\mathbf{U}_f$. The curved arrows indicate the hypothesized circulating directions of the trapped diamagnetic particles.

3.4 Results and Discussion

3.4.1 Particle Concentration

Figure 10 shows the top-view images of 5 μm polystyrene particles during magnetic concentration at the leading edge of the two attracting magnets with respect to the ferrofluid flow. Allowing for the experiment to run, these snapshots were obtained under a continuous bright-field illumination at five-minute increments, starting with the initial time of 5 s. It is important to note that fluorescent labeling of particles is usually required for visualization purposes of particles suspended in ferrofluids [21,27,29,30,77]. This is, however, not necessary in this experiment due to the diluted state of the solution. The magnet-magnet distance is 2.2 mm including the 2 mm thick PDMS and the 200 μm thick cover slip. The average flow speed is 2 mm/s, at which very few particles (<5% in number) were observed to escape from the downstream side of the magnets. It was

estimated through theoretical calculation based on the measured liquid height difference in the inlet and outlet reservoirs [77] and also verified by tracking individual particles in the inlet section of the microchannel that is distant from the stronger magnet field closer to the magnets edge.

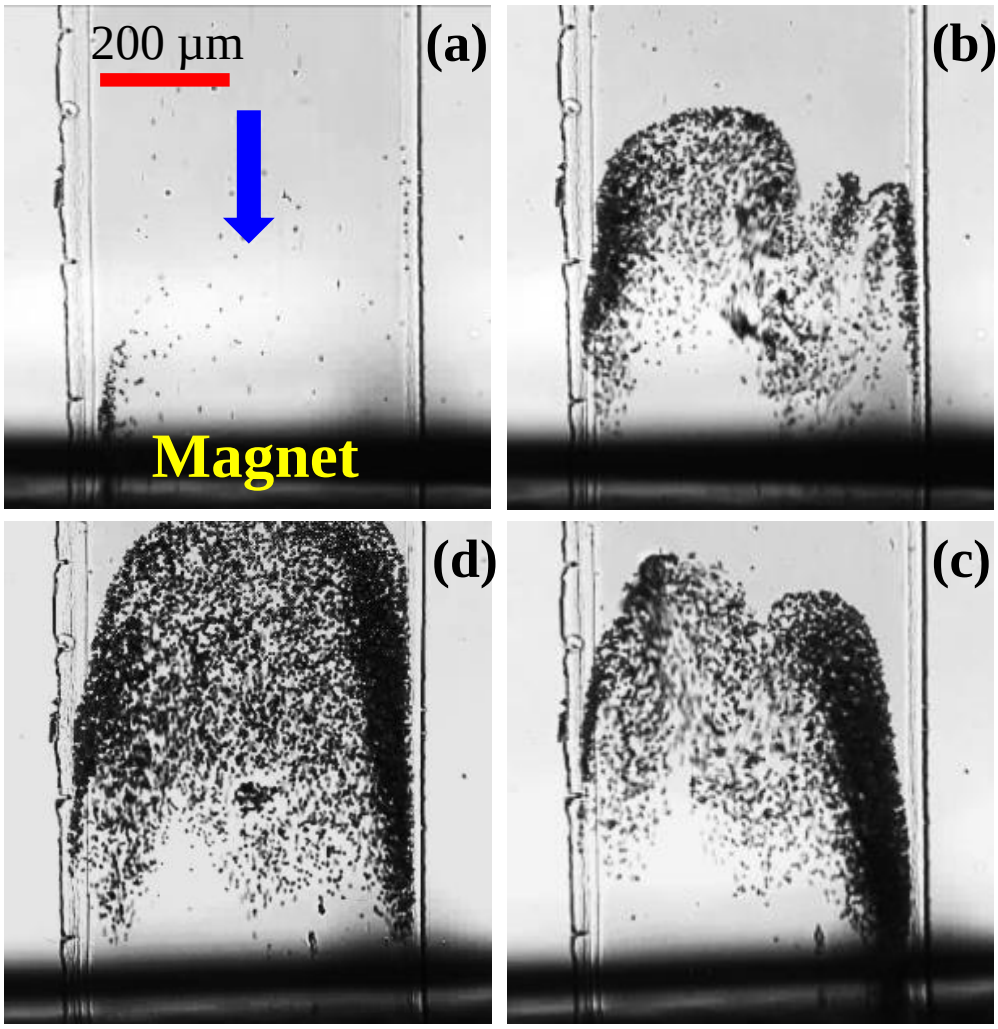

Figure 10: Snapshot images demonstrating the development of magnetic concentration of 5 µm polystyrene particles in 0.05× EMG 408 ferrofluid flow after 5 s (a), 5 minutes (b), 10 minutes (c), and 15 minutes (d). The magnet-magnet distance is 2.2 mm and the average flow speed is 2 mm/s. The block arrow in (a) indicates the flow direction.

As predicted, polystyrene particles are magnetically trapped and continuously concentrated in the ferrofluid in front of the leading edge of the attracting magnets by

negative magnetophoresis. However, wave-like chaotic motions are observed for the trapped particles, which is evident in Figure 10 (see images (b) and (c)). This is beyond our expectation considering the fact of low-Reynolds number (computed as 0.2) in the tested flow. It is speculation that it may be a consequence of the misaligned magnets that can take place in two circumstances: one is that the two magnets themselves are not aligned with their centers being shifted, and the other is that either or both of the two magnets are not placed symmetrically with respect to the microchannel. If neither of these misalignments occurs, however, diamagnetic particles can be magnetically concentrated in two nearly symmetrically distributed circulations relative to the channel centerline (see Figure 12). In addition, one can see from Figure 10 that the particle trapping zone is extended to upstream when more and more particles are accumulated. This may be simply because particles need to take a larger space for further accumulation.

3.4.2 Magnet Distance and Flow Speed Effects

The magnet–magnet distance effect on the magnetic concentration of 5-μm polystyrene particles was studied by varying the thickness of the PDMS slab. The maximum average flow speed of 0.05 × EMG 408 ferrofluid, at which the magnetic concentration of all flowing particles can still be achieved, was measured for three values of PDMS thickness (1, 2, and 5 mm). Also recorded were the minimum ferrofluid flow speeds at which no particles can be trapped for various PDMS thicknesses. A line graph of these two relationships is presented in Figure 11a, which, as expected, demonstrates an increasing flow speed (and hence a greater particle throughput) at a smaller magnet–

magnet distance for both circumstances. More importantly, Figure 11(a) can work as a phase diagram for diamagnetic particle concentration, where the two lines divide the diagram into three distinct regions, i.e., complete trapping, partial trapping and zero trapping. Figure 11(b1–b3) illustrates the snapshot images of the concentrated particles 10 min after the running of the experiment for each of the three PDMS thicknesses. An apparently greater trapping zone is observed for a larger magnet–magnet distance. This may be attributed to the reduced effect of confining magnetic field lines in between two magnets with a larger separation gap, and so the magnetic field gradients can extend to a farther distance outside of the magnets.

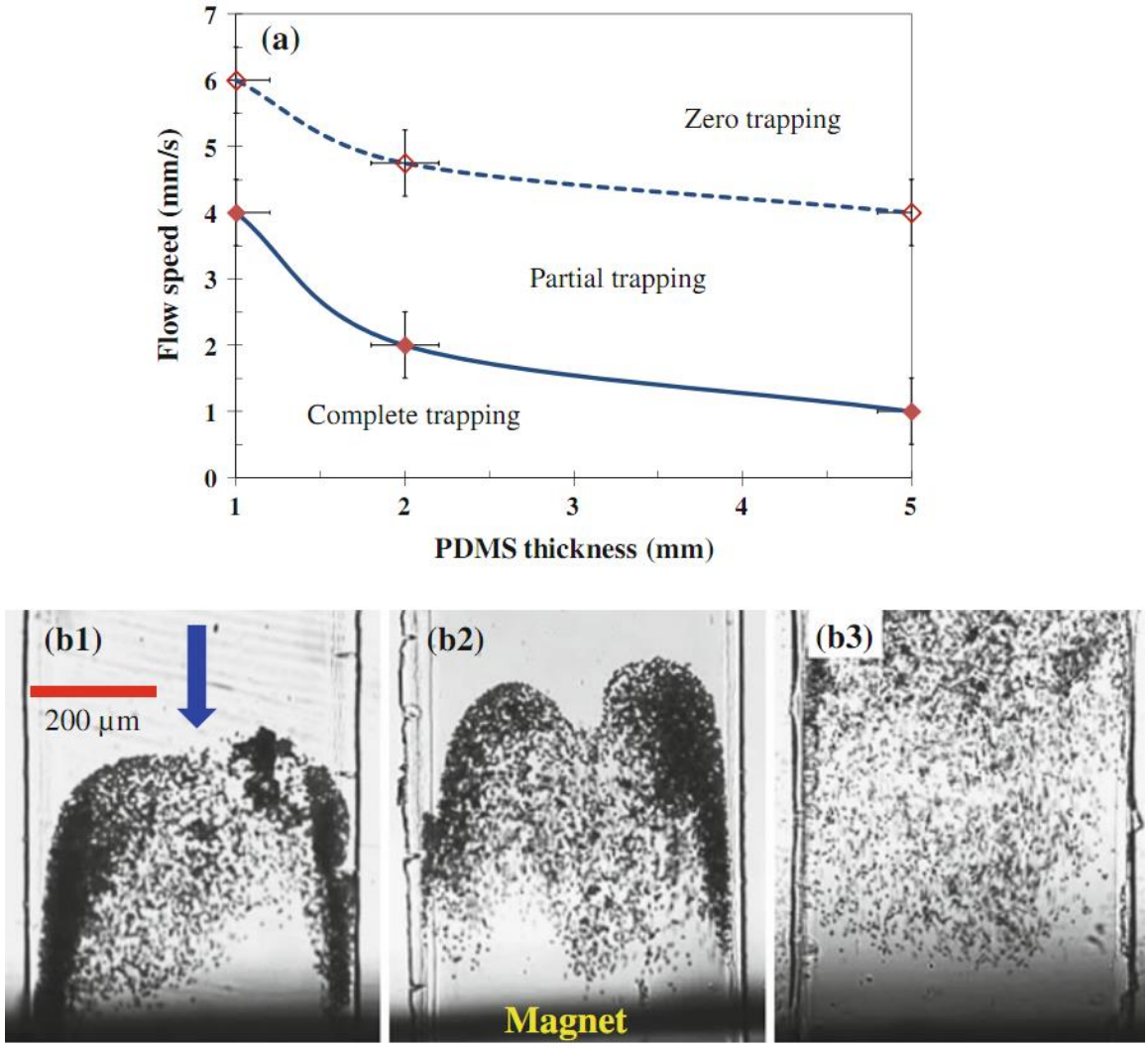

Figure 11: (a) Phase diagram illustrating the magnet–magnet distance (controlled by the thickness of the PDMS slab) effect on the magnetic concentration (reflected by the flow speed) of 5 µm polystyrene particles in 0.05 × EMG 408 ferrofluid. The two lines represent the measured ferrofluid flow speeds at which all (solid line with filled symbols) and no (dashed line with hollow symbols) particles can be trapped, respectively. Error bars are included for experimental data (symbols). The lines are used only for guiding the eyes. (b) Snapshot images of concentrated particles (each was taken 10 min after conducting the experiment) for the three tested magnet–magnet distances. The block arrow in (b1) indicates the flow direction.

The flow rate effect on diamagnetic particle concentration was observed by decreasing the ferrofluid flow speed from the above-determined maximum value for the case with a 2-mm thick PDMS. It was found that the flow effect on the location of particle trapping zone is insignificant. This may be because the magnetophoretic particle velocity decays very quickly from the edge of the magnets, which is clearly indicated by the arrow plots in Figure 9. However, the number of trapped particles decreases at a smaller ferrofluid speed within the same amount of concentration time because less particles travel into the channel with the flow.

3.4.3 Live Yeast Cell Concentration

Figure 12(a) shows a snapshot image of live yeast cells after 10 minutes of continuous concentration in 0.05× EMG 408 ferrofluid. The microfluidic device is similar to that used in Figure 10 with a magnet-magnet distance of 2.2 mm. The magnetic concentration was implemented at an average ferrofluid flow speed of 2 mm/s, which is identical to that for concentrating 5 μm polystyrene particles in the same device. This is reasonable considering that the live yeast cells used have diameters of 3-5 μm on average. However, distinct from the wave-like dynamic motions for the trapped particles in Figure 10, the yeast cells appear to be accumulated inside two nearly symmetric circulations as demonstrated in Figure 12(a). As noted above, the latter phenomenon is attributed to the precise alignment of the two attracting magnets with respect to each other and to the microchannel as well. However, the circulating directions of the trapped yeast cells here (see curved arrows) are opposite to our hypothesized directions. The reason behind this is currently unclear, which needs a further investigation that considers

the complex cell-fluid interactions, with also the consideration of the magnetic nanoparticles in suspension. The two magnets can be easily removed during the experiment, after which the concentrated particles and cells were observed to be washed out by the ferrofluid flow easily. Figure 12(b) shows a snapshot of thus released yeast cells, which demonstrates the flexibility of this magnetic concentration technique.

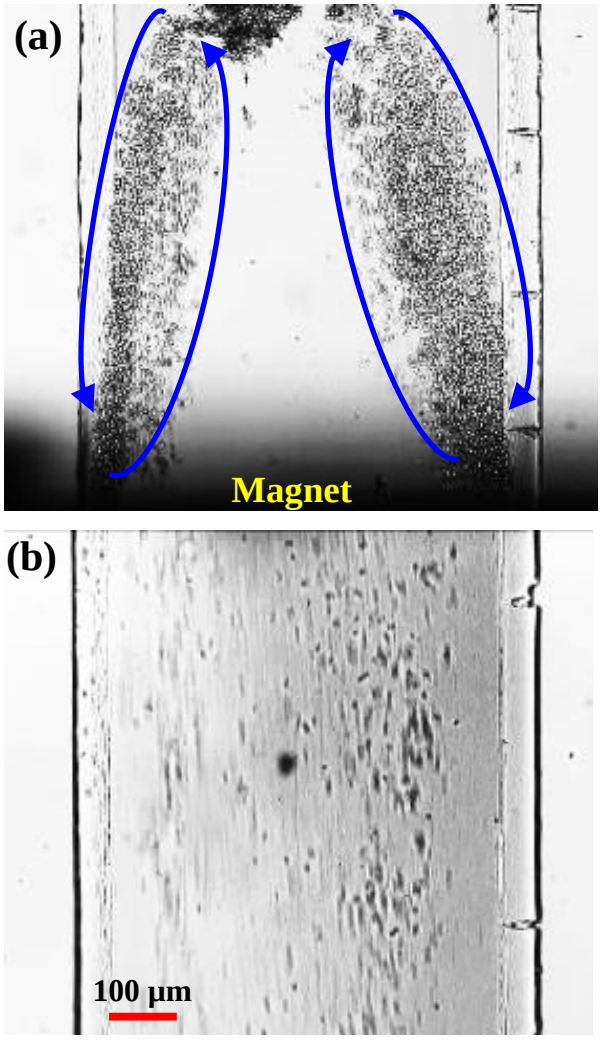

Figure 12: Snapshot images of magnetically concentrated yeast cells in 0.05× EMG 408 ferrofluid (a) and released yeast cells when the magnets are removed (b). The average flow speed is 2 mm/s and the magnet-magnet distance is 2.2 mm, which is identical to those in Figure 10 for 5 µm polystyrene particles. The arrows in (a) highlight the two nearly symmetric circulations in which yeast cells are magnetically trapped. The flow direction is downward in both images.

A biocompatibility test was also conducted by comparing the ratio of live to dead yeast cells before and after the experiment using a spread plate technique. In brief, 100 µl of the diluted cell suspension was plated in triplicates on potato dextrose agar plates. After cell incubation at 30 °C for 24–48 h, the colonies were counted and the CFU/ml (colony forming unit) was determined. A slight decrease (around 5 %) in the cell count was observed, which indicates that the exposure to dilute ferrofluid and magnetic force has negligible influences on the viability of yeast cells. Further experiments will be done to test the biocompatibility of this ferrofluid-based magnetic concentration approach with vulnerable cells like mammalian cells.

3.5 Summary

Here, a simple technique for magnetic concentration of diamagnetic particles in ferrofluid flow through a straight microchannel using two attracting magnets was developed. As they are placed on the top and bottom of the microfluidic device and held in position by the natural attractive force, these magnets can be readily removed during and after experiments. Moreover, by using a glass cover slip and a thin layer of PDMS to decrease the magnet-magnet distance, the suspending ferrofluid can be significantly diluted and so bright field illumination is sufficient for particle visualization. Such a magnetic/fluorescent label-free particle handling technique has been demonstrated by concentrating 5 µm polystyrene particles and live yeast cells in 0.05× EMG 408 ferrofluid. The effects of ferrofluid flow speed and magnet-magnet distance on the concentration performance are examined for polystyrene particles. The evidence of the

magnetic concentration of yeast cells without significant biological harm proves that it can be useful for bio applications where bio-particle enrichment is required.

CHAPTER 4

SEPARATION

4.1 Background

Separating particles and cells from a mixture is often necessary in many biological related applications [15]. In most recent studies, a variety of methods are used for particle separation including electric [16,109], magnetic [17,43], acoustic [110,111], and optical [112,113] forces [14,114-116]. As the magnetic approach proves to be simplest and cheapest, studies have been conducted involving the separation of magnetically tagged objects from that of non-magnetic materials [17,42,43]. This need for magnetic labeling is difficult as it requires manual tagging of each micro-particle used. This problem is absent in light of utilizing negative magnetophoresis for nonmagnetic or diamagnetic particle handling.

Many studies have demonstrated success in diamagnetic particle manipulation suspended in paramagnetic solution [10,33,44,72,77]. This approach suffers from complications as the magnetization of paramagnetic salt solutions is weak and thus stimulates slow rates of particle deflection. Consequently, increasing the salt concentration resolves this issue, however, biocompatibility problems arise [10]. These issues are not encountered when using ferrofluids, which provide a relatively higher order of magnetization.

Mao's group has conducted studies involving diamagnetic particle separation within a continuous ferrofluid flow under the phenomenon of negative magnetophoresis,

however, their study require a separation buffer stream [27,28]. Prior to the actual enactment of deflection, particles suspended within its medium must first be restrained by a co-flowing buffer medium. The use of separate flows for particle separation proves troublesome as it requires more complicated microchannel configurations, less control of the overall flow behavior, and forces the particles to experience different aqueous environments within the same device. The work involved in this chapter does not required this sheath stream as one magnet provides focused particle stream while another magnet induces a size-based separation of the particle mixture.

This work produces a simple technique for size-based diamagnetic particle separation in dilute ferrofluid flow through a straight microchannel utilizing a pair of magnets. Imbedding both magnets along the device, the first magnet is fixed where it can provide full deflection for the particle mixture against one side of the channel wall while a second magnet allows for the separation of particle based on their diameters. Once realizing this concept using artificial polystyrene particles, the separation mechanism is applied to separate live yeast cells from a larger polystyrene particle mixture. Moreover, an analytical model is created to provide support for simulation and verification.

4.2 Experiment

Standard soft lithography method was used to fabricate the straight microchannel. Detailed procedures for channel fabrication can be referred to in Appendix A. The rectangular-cross sectioned microchannel dimensions consist of a length of 2 cm, 200 μm width, 25 μm depth, and 5 distinct branches at each of the two reservoirs. By utilizing these branches, created by four rectangular blocks, the separation result can be

distinguishably visualized. Two equal and opposing Neodymium-Iron-Boron (NeFbB) permanent magnets (B221, 1/8" × 1/8" × 1/16", K&J Magnetics Inc.) were imbedded with the magnetization directions perpendicular towards the microchannel side-walls. Shown in Figure 13, the device has its first magnet placed 500 μm away from the microchannel, edge to edge, while the distance of the second magnet is varied based on experimental requirements.

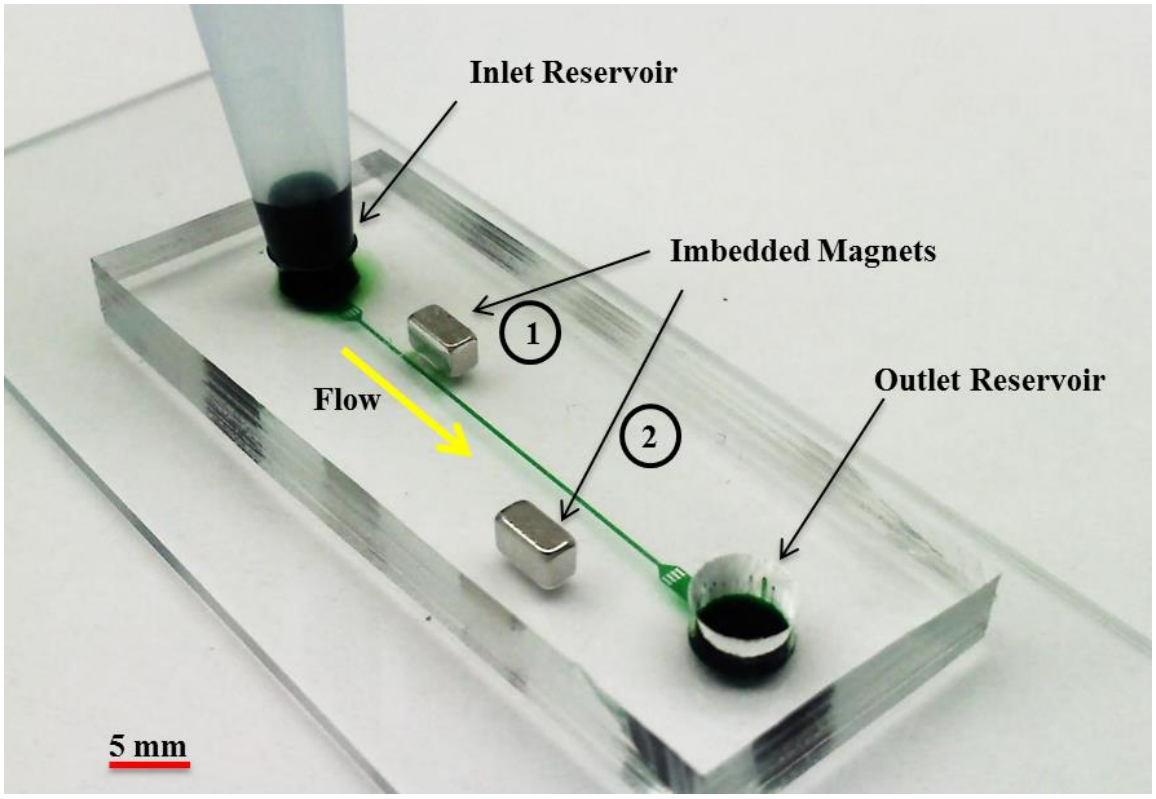

Figure 13: Picture of the separation experimental microfluidic device with the microchannel and reservoirs filled with green food dye for clarity. Physical branches at the reservoirs allow for more distinction while visualizing the results of the separation. In this image, the first magnet is positioned at about 500 μm to the microchannel side while the second magnet is placed 2600 μm away from the opposite channel edge.

A commercially available water-based ferrofluid, EMG 408 (Ferrotec Corp.), was obtained and diluted 0.05× its original 1.2% magnetic nanoparticle (10nm diameter)

concentrated suspension. To show evidence of size-based separation, 3 and 10 μm polystyrene particles (Thermo Fisher Scientific) were suspended at a concentration of 5×10^6 and 4×10^5 particles/ml, respectively. Live yeast cells (*Saccharomyces cerevisiae*) were cultured overnight in Sabouraud's dextrose broth in a shaker incubator at 30 °C, and were re-suspended in sterile phosphate buffered saline (PBS) solution to a concentration of 6.85×10^8 cells/ml. Prior to use, live yeast cells were washed with de-ionized water three times and re-suspended in 0.05× EMG 408 ferrofluid to a final concentration of around 5×10^6 cells/ml and mixed with similar concentration for the 10 μm particles as mentioned above. The measured diameter of yeast cells is 5 μm in approximation. Tween 20 (Fisher Scientific) was added to both the particle and cell suspensions at 0.1% by volume to minimize their aggregations and adhesions to both microchannel walls and towards other particles.

The microchannel was rinsed thoroughly after its fabrication and prior to experiment. A standard 1-ml pipette tip was used to elevate the inlet fluid height in order to produce a pressure driven flow (see Figure 13). Adjusting this height provides control to an approximation of the fluid flow speeds. To reduce the effects of back-flow, the outlet reservoir was manually kept free of fluid buildup during experimentation with the use of a pipette. Particle/cell motion was visualized using an inverted microscope (Nikon Eclipse TE2000U, Nikon Instruments, Lewisville, TX) under a bright-field illumination. Digital videos (at a time rate of around 12 frames per seconds) and images were recorded through a CCD camera (Nikon DS-Qi1Mc) and post-processed using the Nikon imaging software (NIS-Elements AR 2.30).

4.3 Theory

4.3.1 Mechanism

Diamagnetic particles undergo negative magnetophoresis in a ferrofluid when subjected to a non-uniform magnetic field. This motion, $\mathbf{U}_m$, points in the direction of decreasing magnetic field and is expressed by [21,75],

$$\mathbf{U}_m = \frac{-\mu_0 \phi a^2}{9\eta f_D} \frac{M_d L(\alpha) \nabla \mathbf{H}^2}{H} \tag{8}$$

$$L(\alpha) = \coth(\alpha) - \frac{1}{\alpha} \quad \text{and} \quad \alpha = \frac{\pi \mu_0 M_d H d^3}{6 k_B T} \tag{9}$$

where μ_0 is the permeability of free space, ϕ is the volume fraction of magnetic nanoparticles in the ferrofluid, a is the radius of diamagnetic particles, η is the ferrofluid viscosity, f_D is the drag coefficient to account for the particle-wall interactions [21,29,30,73,77], M_d is the saturation moment of magnetic nanoparticles, $L(\alpha)$ represents Langevin function [108], $\mathbf{H}$ is the magnetic field with a magnitude of H, d is the average diameter of magnetic nanoparticles, k_B is the Boltzmann constant, and T is the ferrofluid temperature. Note regarding equation (8) that the magnetized influence from that of the diamagnetic particles is overlooked due to its negligent contribution while suspended in ferrofluid [17,43,24].

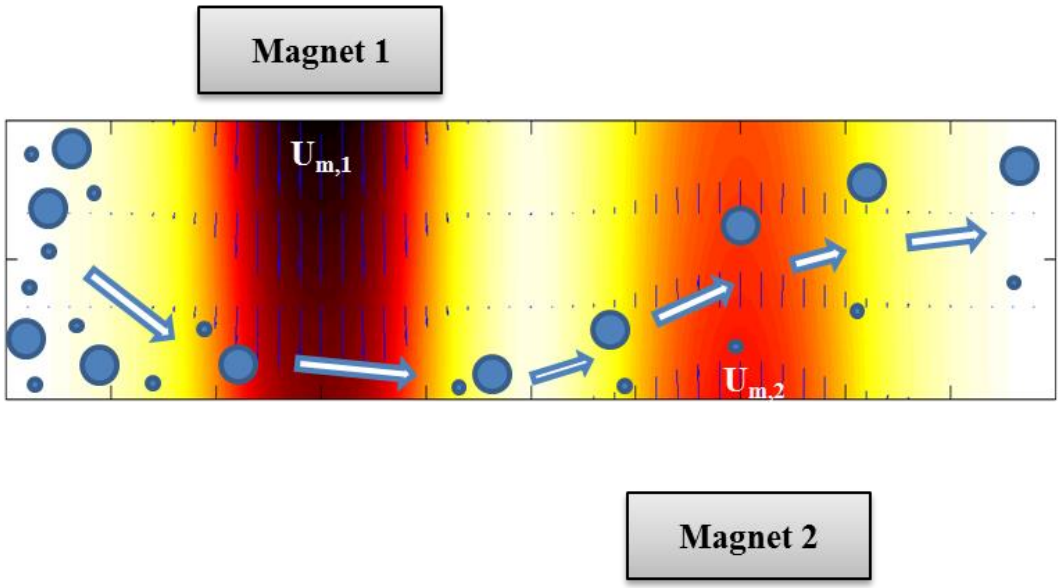

Figure 14: Illustration of the mechanism for magnetic separation of diamagnetic particles in a pressure-driven ferrofluid flow through a straight microchannel using two permanent magnets. The background color indicates the magnetic field contour (the darker color, the larger magnitude). The arrows display the expected trajectory of the particles. Particles experience full deflection passing through the first magnetic field and then, due to the weaker 2nd magnetic field, the larger particles deflect further, thus producing separation between our two sized particles.

By using two magnets in a manner catered towards more precise particle deflection, the work of Liang et al. [21] can be extended for use in size-based particle separation. Realizing that the magnetic force experienced by a particle is proportional to its volume, different positions of set magnets can be implemented to deflect various particle sizes independently. Figure 14 shows the separation mechanism. The magnetic field contours were created by computing Furlani's analytical formula [88] which is also detailed in Liang et al. [21]. Assuming a consistent mixture of ferrofluid and diamagnetic particles, the effects of the particle's on that of the ferrofluid is neglected. With the two different sized particles only differing in diameter (equal magnetization), a magnetic field gradient would always provide a stronger force magnitude on the larger sized or volume

particle, inducing a farther rate of deflection than that of the smaller particle. Providing slow flow speeds enhances this deflection while increasing flow speeds minimize it. As the two magnets are fixed once imbedded and the overall flow speed of the length of the channel cannot be varied, precise parameters can be used to produce size-based particle separation. At ideal conditions, the mixture of particles passing through the closer first magnet should experience full deflection within the microchannel width. After passing by the 1st magnetic field, the particle mixture follows its straight path line along the channel wall.

Successively, once the full deflection is realized, the method of separation can be achieved by the 2nd magnet. Entering the second and weaker magnetic field, the magnetic force should be noticeably discriminatory towards the size of the particles and, therefore, deflecting the larger particle farther than compared to the smaller. This was accomplished by placing the 2nd magnet further away, approximately 5 times farther.

4.3.2 Simulation

According to above analysis, a 3D analytical model was developed to simulate the trajectory of diamagnetic particles in ferrofluid flows within this rectangular cross-sectioned microchannel. The instantaneous position of a particle, $\mathbf{r}_p$, was obtained by integrating the particle velocity over time,

$$\mathbf{r}_p = \mathbf{r}_0 + \int_0^t \left[\mathbf{U}_f(t') + \mathbf{U}_m(t') \right] dt' \tag{10}$$

where $\mathbf{r}_0$ is the initial position of the particle, and t is the time coordinate. The fluid velocity, $\mathbf{U}_f$, and magnet force induced velocity, $\mathbf{U}_m$, are dependent on position and so

vary with time during the particle migration. The contribution of gravity to particle velocity is excluded in equation (10) as explained above. Inertia is also neglected as both the calculated fluid and particle Reynolds numbers are much smaller than 1 within the experimental conditions. The ferrofluid flow in the straight microchannel was assumed fully developed and not affected by particle magnetophoresis. The flow velocity was assumed to follow the analytical formula for pressure-driven flow in a rectangular channel [77]. A custom-written Matlab® program was employed to determine the particle position with respect to time and to plot the particle trajectory, which was described in detail in an earlier work [21].

4.4 Results and Discussion

4.4.1 Particle Separation

Shown in Figure 15, the size-based separation of 3 and 10 μm polystyrene particles were studied and continuously separated at 0.05× EMG 408 ferrofluid at a designated flow speed of 0.6 mm/s. With magnets 1 and 2 placed 500 μm and 2600 μm, respectively, away from the microchannel, the inlet and outlet of the device were recorded along with four particular positions of interest while the experiment ran. As evident in Figure 15(b), the inlet view shows a mixture of both sized particles flowing into the microchannel with scattered positioning relative to the channel width while Figure 15(c), the outlet, shows the same binary mixture of particles flowing away from the main length of the microchannel and into distinct and separate branches. Note that the images taken from experiment were cropped and altered, in brightness and contrast, to

better visualize these micron-sized particles. The provided superimposed images were obtained directly from recorded video evidence.

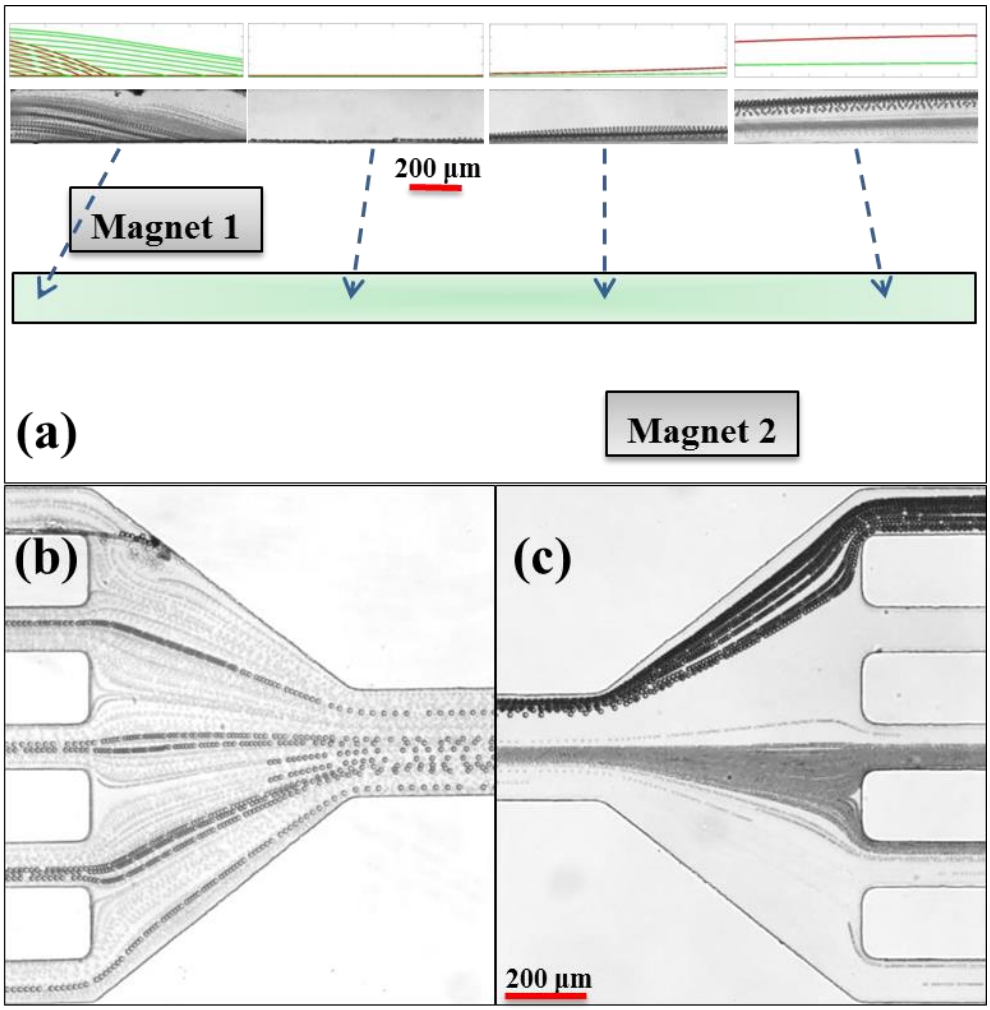

Figure 15: Experimental superimposed mages demonstrating the development of magnetic separation of 3 µm and 10 µm polystyrene particles in 0.05× EMG 408 ferrofluid flowing at 0.6 mm/s. Magnet 1 and 2 are placed 500 µm and 2600 µm away, edge to edge, from the microchannel, respectively. Superimposed images showing the inlet and outlet correspond to (b) and (c), respectively. At the locations specified by dotted arrows, (a) describes the process of size-based particle separation with the top row of images from our analytical solution while below it are superimposed experimental images. In the analytical solution, the red lines represent the 10 µm particles while the green represent the 3 µm particles.

Figure 15(a) shows the process of particle separation in detail with relative magnet positions for reference. The first window is located at the leading edge of the first

magnet, the second window shows the particle behavior downstream after the rear edge of the first magnet but far before the leading edge of the second magnet, the third window shows the beginning of the separation process at the leading edge of the second magnet, and finally, the fourth window presents the view of separated particles after the rear edge of the second magnet. Following the sequence described in the separation mechanism section, the polystyrene particles experience negative magnetophoretic deflection by both positioned magnets with the first magnet acting to fully deflect both particles while the second magnet provides the means to deflect the larger particles further than those smaller. Experimental superimposed images are shown in the lower row while the top row is images taken from particle tracking with our analytical solution. Displaying the same trend, the 3 μm particles are represented green while the 10 μm particles are shown as red. Discrepancies between the corresponding images can attribute towards having our flow speeds approximated from the pressure driven flow produced by the liquid height difference.

4.4.2 Flow Speed Effects

The flow speed effects on the particle positions of 3 and 10 μm particles were also studied. Using the same ferrofluid concentration and placing the 1st magnet at 500 μm and the 2nd at 2600 μm, the flow speed was adjusted to 0.6, 0.8, and 1.2 mm/s. The result of this study is shown in Figure 16. Following the previous figures, the blue line represents our calculated result accompanied by experimental data values with included error ranges. Figure 16(b) and 16(c) represents experimental superimposed images of tested cases at 0.6, 0.8, and 1.2 mm/s, respectively. As the trend shows, with an increase

in flow speed, the separation widths between the two particle streams weaken. Verifying the conclusion made earlier with this new set of calculated solution, the separation gap is at its maximum just at the limit where the 10 μm particle gets fully deflected. Here, the simulated results show that exceeding this limit will no longer provide the larger particles with more deflection but rather decrease the separation efficiency by allowing the 3 μm particle be further moved closer towards the same channel side as that of said larger particle.

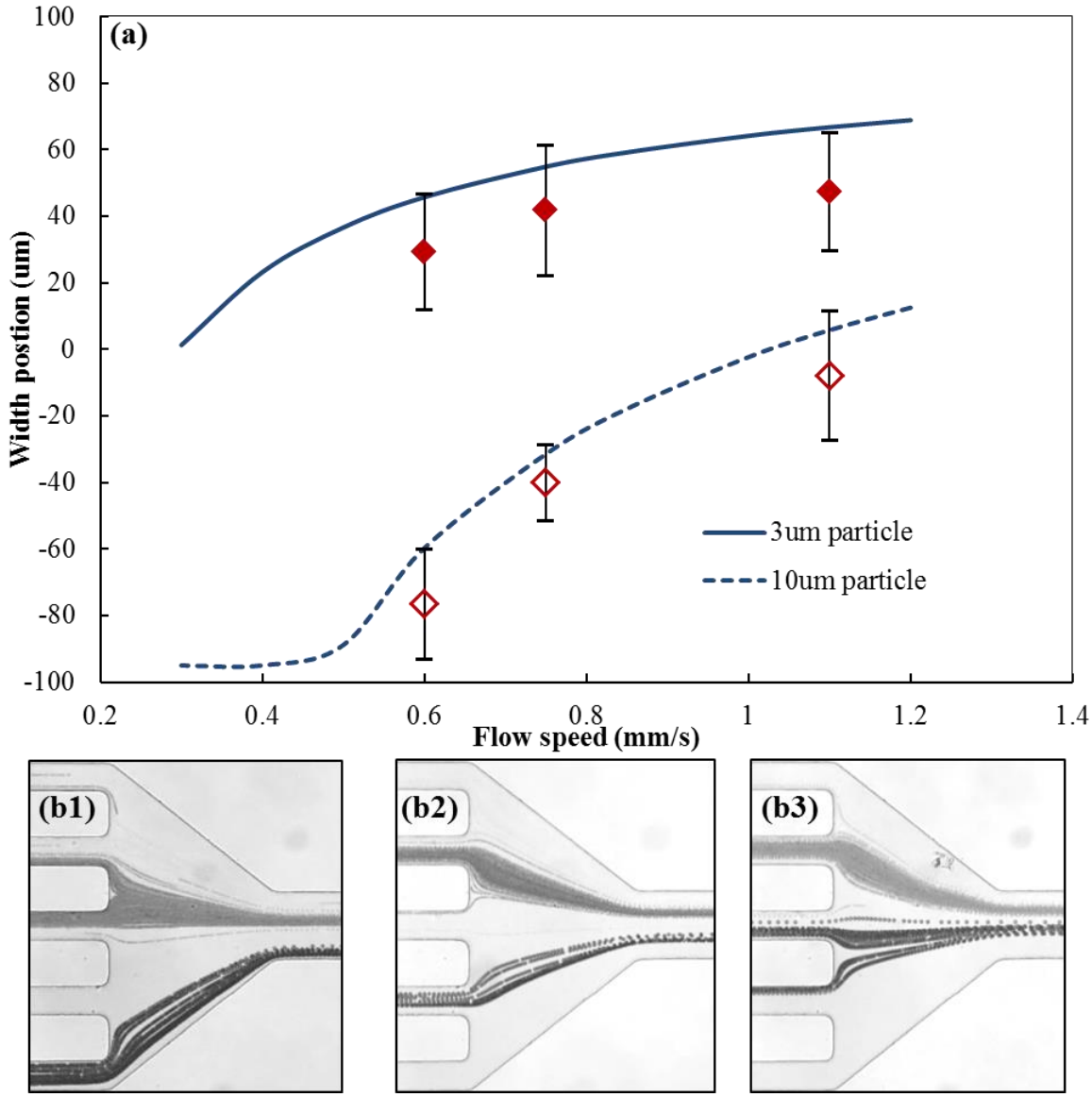

Figure 16: (a) Plot diagram illustrating the flow speed effect on the magnetic separation of 3 and 10 µm polystyrene particles in 0.05× EMG 408 ferrofluid with fixed magnet 1 and 2 positions at 500 and 2600 µm, respectively. The blue lines represent the projected width positions, relative to the channel center, of each of the two particles prior to the branching out of the microchannel while the experimental data are included with error ranges. Superimposed images taken from experiment are also placed here for visual reference with (b1), (b2), and (b3) representing 0.6, 0.8, and 1.2 mm/s flow speeds, respectively.

4.4.3 Magnet Distance Effects

Next, the 2nd or separating magnet's distance effect on the result of the 3 and 10 µm particles' separation gap was examined while fixing the 1st magnet distance at 500 µm. While varying the 2nd magnet distance, the separation behavior differs mostly at the two outlet particle streaming widths. Using a ferrofluid concentration of 0.05× EMG 408 and a set average flow speed of 1.2 mm/s, the experiment was allowed to run and the outlet recorded showing varying separation behavior caused by the 2nd magnet's distance. The result of this study is shown in Figure 4 with the blue line representing our prediction and experimental data with error ranges. The trend shows that with reducing magnet distance, the center-to-center gap between the separated streams of particles increases. With the magnetic deflection of diamagnetic particle at its maximum based on those large particles, it is evident that the ideal condition for a binary mixture of size varying particles' separation is that of one at the threshold condition of the larger particles full deflection after the 2nd magnet. This allows for the bigger particles to be deflected as far as possible while minimizing the rate of deflection the smaller particle travels as a result of experience the same magnetic field.

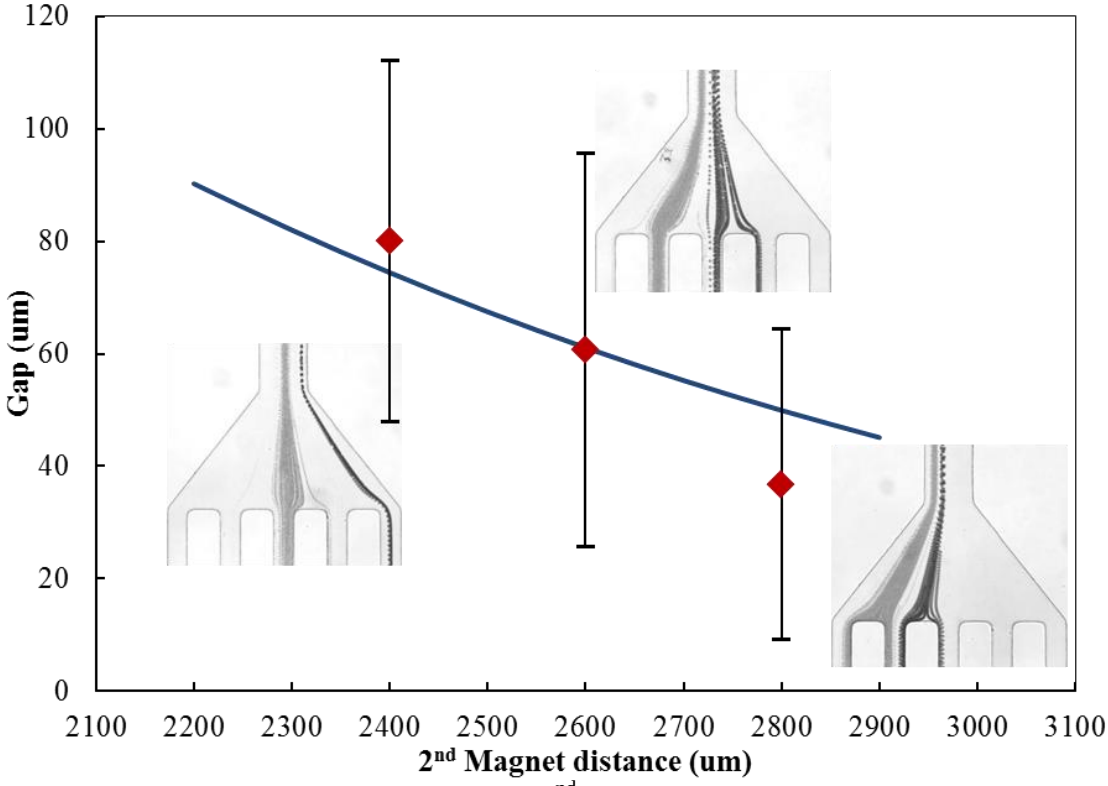

Figure 17: Plot diagram illustrating the 2nd magnet distance effect on the magnetic separation of 3 and 10 µm polystyrene particles in 0.05× EMG 408 ferrofluid at a fixed speed of 1.2 mm/s. The blue line represents the projected center-to-center separation gap between the two particles prior to the branching out of the microchannel while the experimental data are included with error ranges. Superimposed images taken from experiment are also placed here for visual reference.

4.4.4 Live Yeast Cell and Polystyrene Particle Separation

Figure 18 shows a superimposed image of live yeast cells separated from 10 µm polystyrene particles after undergoing the same separation process mentioned before. The left image shows the inlet while the right shows the separation result. The device parameters are similar to that used in our initial study with the 1st and 2nd magnet distance at 500 and 2600 µm, respectively, and an average flow speed of 0.6 mm/s. The smaller images in the lower section shown are the simulated trajectories. The red lines represent 10 µm particles and the green line, the yeast cells. The results prove similar as the

approximate average diameter of yeast cells being 3-5 µm, considering its oval-like shape.

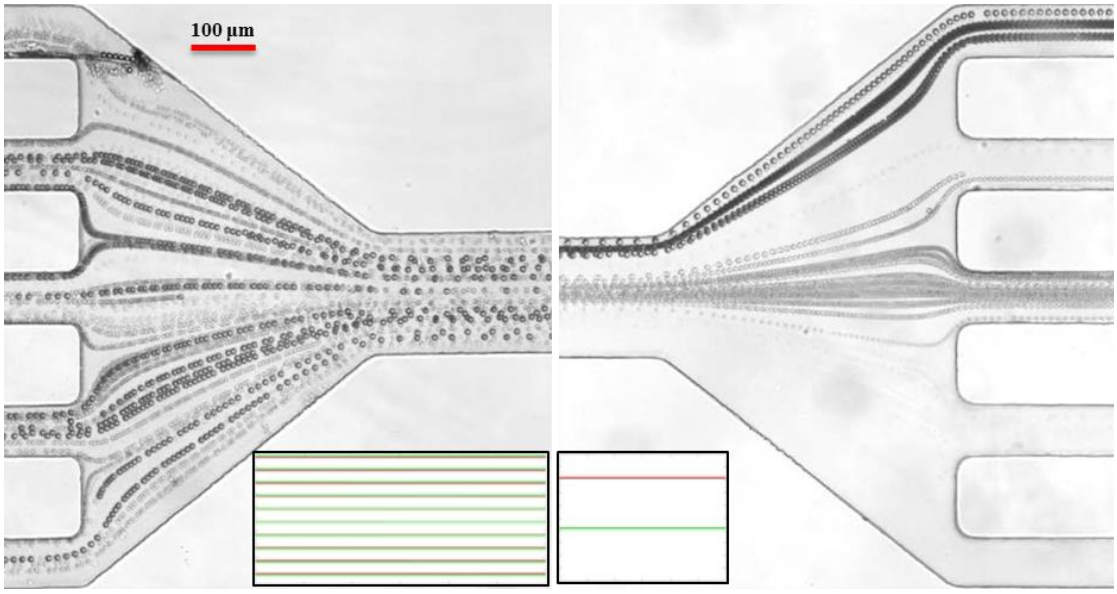

Figure 18: Superimposed image of magnetic separation, at the inlet (left) and outlet (right), of live yeast cells from 10 µm polystyrene particles suspended in ferrofluid at 0.05× EMG 408 dilution with an average flow speed of 0.6 mm/s. Smaller boxes show simulation of the particles' trajectories with 10 µm particles as the red line and yeast cells as the green line. The 1st and 2nd magnets are placed 500 µm and 2600 µm away from the channel edge, respectively.

As successful manipulation of live cells is desired, the methods required for these exploitations must not be detriment towards the individual cell's integrity. As the live yeast cells are suspended in dilute ferrofluid along with artificial polystyrene particles and pressure driven through a microchannel while experiencing negative magnetophoresis, samples were collected and tested for cell viability. In brief, 100 µl of the diluted cell suspension was plated in triplicates on potato dextrose agar plates. After cell incubation at 30 °C for 24–48 h, the colonies were counted and the CFU/ml (colony

forming unit) was determined. While a slight decrease in cell colony count was observed (less than 5%), the results show an overall positive biocompatibility.

4.5 Summary

This chapter provides a simple technique for size-based particle separation of diamagnetic particles suspended in ferrofluid through a straight microchannel using pair magnets by utilizing the mechanism of negative magnetophoresis. Imbedding a pair of permanent magnets, 3 and 10 μm particles were successfully separated. After this concept was proven, studies of varying the flow speed and distance of the magnet responsible for separation were carried out. Additionally, an analytical solution has been developed to predict the behavior of the particles and prove to support experimental findings. The separation optimization, within the scope of our study, was realized once our calculated particle trajectories were compared to that of experimental data trends. Extending our study with live yeast cells, it was found that not only do the cells follow the separation process, the cells were also biocompatible as a result of our experiment.

CHAPTER 5

CONCLUSION AND FUTURE WORK

The manipulation of diamagnetic particles through a ferrofluid filled straight microchannel has been realized utilizing negative magnetophoresis using a pair of permanent magnets. The experimental results here have proven the versatility of exploiting negative magnetophoresis. Most importantly, there is no magnetic tagging of biological cells which are intrinsically diamagnetic in nature. Magnetophoretic induced motion does not create the side effect of fluid heating as observed in the majority of other field force manipulations, namely electric and optical. The device itself does not need any complex channel geometries or any expensive equipment for force field generation and commercially available permanent magnets are very cheap. Furthermore, as observed in the trapping and concentration project, the magnetic field can be turned off by simply the removal of the magnets. This proves the flexible nature of employing magnets for magnetophoretic manipulations of particles.

By taking into consideration the fundamental understanding of magnetophoretic influences on particles, various diamagnetic particle manipulations were realized under the suspension of a commercially available ferrofluid. In chapter 2, the focusing of particles was achieved by symmetrically imbedding two repulsive magnets within our device. This project also provided a novel development of imbedding magnets within PDMS that are repulsive by the configuration of supporting magnets during the device fabrication process. A three-dimensional focusing of 5 μm particles at a flow speed of 0.4 mm/s was accomplished and visualized from the perspective of both the width view and

side view of the microchannel. It was concluded that particle focusing can be enhanced with either decreasing the flow speed, increasing the particle size, or a combination of both. A filtration study was also conducted by running a mixture of 5 μm and 1 μm particles through the device at the same experimental conditions. This study showed the potential application for a magnetic focuser to continuously concentrate and filter mixtures of particles based on size. Additionally, a three-dimensional analytical model was developed and showed good concurrence with respect to the experimental result.

Next, chapter 3 described a method for which particles can be trapped and concentrated using a pair of attracting magnets without the need for imbedding as they are held by their natural attractive force. A glass slide was replaced with a cover slip, which is about 200 μm in thickness, to minimize the distance between the magnets, therefore, strengthening the magnetic field magnitude. This, in turn, allowed for the additional dilution of ferrofluid and provided the visualization through only a bright field view rather than fluorescent. Here, 5 μm particles were trapped and continuously concentrated at varying flow speeds and magnet distances, which controlled by the thickness of the PDMS slab. It was concluded for each magnet-magnet distance, trapping can be categorized into three distinct phases. First, no trapping at high flow speeds. Second, as flow speed is reduced, partial trapping occurs. Lastly, at relatively low speeds, the complete trapping of all particles can be accomplished. Previously used analytical models were unsuccessful in describing the behavior of the concentrated diamagnetic particles due to the negligence of the magnetic nano-particle (ferrofluid) and diamagnetic particle interactions.

Finally, chapter 4 developed a method for a size-based diamagnetic particle separation through a similar straight microchannel using two imbedded magnets. The particle mixture was fully deflected across the width of the microchannel after passing the first magnetic field produced by a relatively closely positioned magnet and then a second, separating magnet, was placed relatively further away to provide a size-based particle separation with respect to the focused particle mixture. 3 μm and 10 μm polystyrene particles were effectively separated in this process and studies varying the flow speed and separating magnet distance were conducted to show their effects on the resulting separation gap. The results showed that, within the constraints of the microchannel (channel width), decreasing separating magnet position or slower flow speeds enhanced the separation gap between the two particle streams. The experimental results were also supported with an analytical model for separation gap predictions.

Once the magnetophoretic manipulation of artificial particles was realized, each of the experimental devices were applied for use with live yeast cells (*Saccharomyces cerevisiae*) at the same successfully implemented experimental conditions. As the polystyrene particles used were 3 μm and 5 μm, the use of yeast cells is acceptable as its sizes range from 3-5 μm. This was found by direct measurement. Furthermore, as biocompatibility is without a doubt required in most processes handling biomaterials, a cell viability test was performed after conducting each of the experiments and proved positive (>90%). This proves to offer bio-applications with a novel way for focusing, concentrating, and separating live cells without adverse effects on biocompatibility.

Mentioned in chapter 3 is the absence of a theoretical model for simulating the particle trapping process. As diamagnetic particles experience negative magnetophoresis, the magnetic nano-particles also experience the same magnetic field with positive magnetophoretic motion. As these magnetic particles accumulate at high magnetic field regions (since the magnet-magnet distance was minimized), there exists an unfavorable effect due to the buildup of nano-particles. There is hypothesis that the accumulation of nanoparticles could, in fact, enhance the diamagnetic particle manipulation, however, this accusation will need to be supported once an accurate numerical simulation is produced and can be compared with experimental results. Students within the research group are currently undertaking the development of this new analytical model for future studies involving these projects.

Further studies regarding these works can contribute to many aspects of improvement. First, this method for continuous particle manipulation can be even more fine-tuned for including smaller cells and other bio materials such as bacteria and virus, which are on the submicron and nanometer scale. These processes can be enhanced through the use of an accurate flow rate producing microfluidic automated pump, optimization of the permanent magnet positions, and even using a multitude of magnets of various strengths tailored to the device. Another concept could include a combination of the studied processes (focusing, concentration, and separation) which can be integrated into one microfluidic device for a potentially higher throughput and applications that require more precise functions. Lastly, a variety of manipulations methods could be incorporated within the same device. For example, this research group is currently

involved in the study of combining electric and magnetic methods where electrophoresis is used to drive the flow while at the same time magnetophoresis manipulates diamagnetic particles in suspension. As the little study has been conducted involving these two force fields in combination, the results are anticipated to further push the boundaries for microfluidic potential and its applications. As modern medical technologies look forward towards the advantages of microfluidics involving the magnetophoretic manipulation of particles, the potential outlook for research and clinical application is excellent.

REFERENCES

[1] Tabeling, P., *Introduction to Microfluidics*. Oxford University Press, 2005.

[2] Squires, T.M., Quake, S.R., *Rev. Modern Phys.*, 2005, 77, 977-1026.

[3] Li, D., *Electrokinetics in Microfluidics*, Elsevier Academic Press, Burlington, MA 2004.

[4] Berthier, J., Silberzan, P., *Microfluidics for Biotechnology*, Artech House, Norwood, MA 2006.

[5] Whitesides, G.M., Nature. 2006, 442, 368-373.

[6] Insight: Lab on a Chip. *Nature*, 2006, 442, 367-418.

[7] Bruus, H., *Theoretical Microfluidics*. Oxford University Press, 2007.

[8] Mark, D., Haeberle, S. Roth, G., von Stetten, F., Zengerle, R., *Chem. Soc. Rev.* 2010, 39, 1153-82.

[9] Church, C., Zhu, J., Wang, G., Tzeng, T.J., Xuan, X., *Biomicrofluidics*, 2009, 3, 044109.

[10] Rodriguez-Villarreal, A.I., Tarn, M.D., Madden, L.A., Lutz., J.B., Greenman, J.B., Samitier, J., Pamme, N., *Lab Chip*, 2011, 11, 1240–08.

[11] Xuan, X., Zhu, J., Church, C., *Microfluid. Nanofluid*,. 2010, 9, 1-16.

[12] Johann, R.M., *Anal. Bioanal. Chem*,. 2006, 385, 408-12.

[13] Nilsson, J., Evander, M., Hammarstrom, B., Laurell, T., *Anal Chimica Acta*, 2009, 649, 141-57.

[14] Pamme, N., *Lab Chip*, 2007, 7, 1644-59.

[15] Ateya, D.A., Erickson, J.S., Howell Jr., P.B., Hilliard, L.R., Golden, J.P., Ligler, F.S., *Anal. Bioanal. Chem.*, 2008, 391, 1485-98

[16] Pethig, R., *Biomicrofluidics* 2010, 4, 022811.

[17] Pamme, N., *Lab Chip* 2006, 6, 24-38.

[18] Friend, J., Yeo, L.Y., *Rev. Mod. Phys.* 2011, 83 647-704.

[19] Erickson, D., Serey, X., Chen, Y.F., Mandal, S., *Lab Chip* 2011, 11, 995-1009.

[20] Zhu, J., Tzeng, T.J., Hu, G. Xuan, X., *Microfluid. Nanofluid.*, 2009, 7, 751-56.

[21] Liang, L., Zhu, J., Xuan, X., *Biomicrofluidics*, 2011, 5, 034110.

[22] Neild, A., S. Oberti, F. Beyeler, J. Dual, B. Nelson, *J. Micromech. Microeng*. 2006, 16, 1562.

[23] Mandal, S., Serey, X., Erickson, D., *Nano Lett.*, 2010, 10, 99–104.

[24] Gijs, M.A.M., *Microfluid. Nanofluid.* 2004, 1, 22-40.

[25] Krebs, M.D., Erb, R.M., Yellen, B.B., Samanta, B., Bajaj, A., Rotello, V.M., Alsberg, E., *Nano. Lett.* 2009, 9, 1812-17.

[26] Kose, A.R., Fischer, B., Mao, L., Koser, H., *Proc. Natl. Acad. Sci. USA* 2009, 106, 21478-83.

[27] Zhu, T.T., Marrero, F., Mao, L.D., *Microfluid. Nanofluid.* 2010, 9, 1003-09.

[28] Erb, R.M., Yellen, B., *Nanoscale Magnetic Materials and Applications*, J. P. Liu ed., 2009, 563-90.

[29] Zhu, T.T., Lichlyter, D.J., Haidekker, M.A., Mao, L., *Microfluid. Nanofluid.*, 2011, 10, 1233-45.

[30] Zhu, T., Cheng, R., Mao, L., *Microfluid. Nanofluid.*, 2011, 11, 695-701.

[31] Kirby, B. J., Micro- and nanoscale fluid mechanics: transport in microfluidic devices, Cambridge University Press 2010.

[32] Yellen, B.B., Hovorka, O., Friedman, G., *Proc. Natl. Acad. Sci.*, 2005, 102, 8860-64.

[33] Peyman, S.A., Kwan, E.Y., Margarson, O., Iles, A., Pamme N., *J. Chromatogr. A*, 2009, 1216, 9055–62.

[34] Friedman, G., Yellen, B.B., *Current Opinion Colloid Interf. Sci,*, 2005, 10, 158-66.

[35] Voltairas, P.A., Fotiadis, D.I., Michalis, L.K., *J. Biomech.*, 2002, 35**,** 813–21.

[36] Lacharme, F., Vandevyver, C., Gijs, M.A.M., *Anal. Chem.* 2008, 80, 2905-10.

[37] Liberti, P.A., Rao, C.G., Terstappen, L.W.M.M., *J. Magn. Magn. Mater.*, 2001, 225, 301-7.

[38] Jordan, A., Scholz, R., Wust, P., Fahling, H., Felix, R., *J. Magn. Magn. Mater.* 1999, 201, 413-19.

[39] Sattel, T.F., Knopp, T., Biederer, S., Gleich, B., Weizenecker, J., Borgert, J., Buzug, T.M., *J. Phys. D: Appl. Phys., 2009, 42, 022001*.

[40] Pankhurst, Q.A., Connolly, J., Jones, S.K., Dobson, J., *J. Phys. D*, 2003, 36, R167-R181.

[41] Pankhurst, Q.A., Thanh, N.K.T., Jones, S.K., Dobson, J., *J. Phys. D: Appl. Phys.*, 2009, 42, 224001

[42] Liu, C.X., Stakenborg, T., Peeters, S., Lagae, L., *J. Appl. Phys.* 2009, 105, 102011-14.

[43] Gijs, M.A.M., Lacharme, F., Lehmann, U., *Chem. Rev.* 2010, 110, 1518-63.

[44] Mirica, K.A., Phillips, S.T., Shevkoplyas, S.S., Whitesides, G.M., *J. Am. Chem. Soc.*, 2009, 131, 10049-58.

[45] Feinstein, E., Prentiss, M., *J. Appl. Phys.* 2006, 99, 064901.

[46] Hu, D., Gu, W., Kamotani, Y., Grotgerg, J.B., Takayama, S., *Physiol. Meas.*, 2005, 26, R73-98.

[47] Fu, L.M., Yang, R.J., Lin, C., Pan, Y., Lee, G., *Anal. Chim. Acta.*, 2004, 507, 163-9.

[48] Chang, C., Huang, Z., Yang, R.J., *J. Micromech. Microeng.*, 2007, 17, 1479-86.

[49] Tsai, C.H., Hou, H.H., Fu, L.M., Microfluid. Nanofluid., 2008, 5, 827-36.

[50] Hong, T.F., Ju, W.J., Wu, M.C., Tai, C.H., Tsai, C.H., Fu, L.M., *Microfluid. Nanofluid.*, 2010, 9, 1125-33.

[51] Lee, H.C., Hou, H.H., Yang, R.J., Lin, C.H., Fu, L.M., *Microfluid. Nanofluid.*, 2011, 11, 469-78.

[52] Watkins, N., Venkatesan, B.M., Toner, M., Rodriguez, W., Bashir, R., *Lab Chip*, 2009, 9, 3177-84.

[53] Chung, T.D., Kim, H.C., *Electrophoresis*, 2007, 28, 4511-20.

[54] Godin, J., Chen, C., Cho, S.H., Qiao, W., Tsai, F., Lo, Y.H., *J. Biophoton*, 2008, 1, 355-76.

[55] Mao, X., Huang, T., *IEEE Nanotechnol. Mag.*, 2008, 2, 22-7.

[56] Zhao, Y., Fujimoto, B.S., Jeffries, G.D.M., Schiro, P.G., Chiu, D.T., *Opt. Express*, 2007, 15, 6167-76.

[57] Petersson, F., Nilsson, A., Jonsson, H., Laurell, T., *Anal. Chem.*, 2005, 77, 1216-21.

[58] Shi, J., Yazdi, S., Lin, S.S., Ding, X., Chiang, I.K., Sharp, K., Huang, T.J., *Lab Chip*, 2011, 11, 2319-24.

[59] Liang, L., Qian, S., Xuan, X., *J. Colloid Interface Sci.*, 2010, 350, 377-9.

[60] Yu, C.H., Vykoukal, J., Vykoukal, D.M., Schwartz, J.A., Gascoyne, P.R.C., *J. Microelectromech. Syst.*, 2005, 14, 480-7.

[61] Chu, H., Doh, I., Cho, Y., *Lab Chip*, 2009, 9 686-91.

[62] Bhagat, A.A.S., Kuntaegowdanahalli, S.S., Papautsky, I., *Biomed. Microdevices.*, 2010, 12, 187-95.

[63] Di, C.D., Irimia, D., Tompkins, R.G., Toner, M., *Proc. Natl Acad. Sci.*, 2007, 104, 18892-7.

[64] Choi, S., Song, S., Choi, C., Park, J.K.,*Small*, 2008, 4, 634-41.

[65] Aoki, R., Yamada, M., Yasuda, M., Seki, M., *Microfluid. Nanofluid.*, 2009, 11, 266-73.

[66] Leshansky, A.M., Bransky, A., Korin, N., Dinnar, U., *Phys. Rev. Lett.*, 2007, 98, 234501.

[67] Yang, S., Kim, J.Y., Lee, S.J., Lee, S.S., Kim, J.M., Lab Chip, 2011, 11, 266-73.

[68] Church, C., Zhu, J., Nieto, J., Keten, G., Ibarra, E., Xuan, X., *J. Micromech. Microeng.*, 2010, 20, 065011.

[69] Zhu, J., Xuan, X., *Electrophoresis*, 2009, 30, 2668-75.

[70] Nguyen, N.T., *Microfluid Nanofluid.*, 2012, 12, 1-16.

[71] Suwa, M., Watarai, H., *Anal. Chim. Acta.*, 2011, 690, 137-47.

[72] Shen, S., Hwang, H., Hahn, Y.K., Park, J.K., *Anal. Chem.*, 2012, 84, 3075-81.

[73] Vojtisek, M., Tarn, M.D., Hirota, N., Pamme, N., *Microfluid Nanofluid.*, 2012, 13, 625-35.

[74] Afshar, R., Moser, Y., Lehnert, T., Gijs, M.A.M., *Anal. Chem.*, 2011, 83, 1022-9.

[75] Liang, L., Xuan, X., *Microfluid Nanofluid.*, 2012, 13, 637-43.

[76] Kose, A.R., Koser, A., *Lab Chip*, 2012, 12, 190-6.

[77] Zhu, J., Liang, L, Xuan, X., Microfluid Nanofluid., 2012, 12, 65-73.

[78] Zhu, T., Cheng, R., Lee, S.A., Rajaraman, E., Eiteman, M.A., Querec, T.D., Unger, E.R., Mao, L., Microfluid Nanofluid., 2012, 14, 645-54.

[79] Rosensweig, R.E., *Ferrohydrodynamics*. Cambridge University Press, 1985.

[80] Furlani, E.P., Permanent Magnet and Electromechanical Devices: Materials, Analysis, and Applications, New York Academic, 2001.

[81] Pratt, E.D., Huang, C., Hawkins, B.G., Gleghorn, J.P., Kirby, B.J., *Chem Engineering Sci.*, 2011, 66, 1508-22.

[82] Ghubade, A., Mandal, S., Chaudhury, R., Singh, R.K., Bhattacharya, S., *Biomed. Microdev.*, 2009, 11, 987-95.

[83] Hamblin, M.N., Xuan, J., Maynes, D., Tolley, H.D., Belnap, D.M., Woolley, A.T., Lee, M., Hawkins, A.R., *Lab Chip*, 2010, 10, 173-8.

[84] Lapizco-Encinas, B.H., Rito-Palmomares, M., *Electrophoresis*, 2007, 28, 4521-38.

[85] Santana, S.M., Liu, H., Bander, N.H., Gleghorn, J.P., Kirby, B.J., *Biomed. Microdev.*, 2012, 14, 401-7.

[86] Warkiani, M.E., Lou, C.P., Liu, H., Gong, H.Q., *Biomed. Microdev.*, 2012, 14, 669-77.

[87] Zheng, S., Lin, H.K., Lu, B., Williams, A., Datar, R., Cote, R.J., Tai, Y.C., *Biomed. Microdev.*, 2011, 13, 203-13.

[88] Church, C., Zhu, J., Huang, G., Tzeng, T.R., Xuan, X., *Biomicrofluid*, 2010, 4, 044101

[89] Jen, C.P., Chen, T.W., *Biomed. Microdev.*, 2009, 11, 597-607.

[90] Lapizco-Encinas, B.H., Simmons, B.A., Cummings, E.B., Fintschenko, Y., *Anal. Chem.*, 2004, 76, 1571-9.

[91] Lapizco-Encinas, B.H., Davalos, R.V., Simmons, B.A., Cummings, E.B., Fintschenko, Y., *J. Microbiol. Methods*, 2005, 62, 317-26.

[92] Ohta, A.T., Chiou, P.Y., Wu, M.C., *J. Microelectromech Sys.*, 2007, 16, 491-9.

[93] Sabounchi, P., Morales, A.M., Ponce, P., Lee, L.P., Simmons, B.A., Davalos, R.V., *Biomed. Microdev.*, 2008, 10, 661-70.

[94] Shafiee, H., Caldwell, J.L., Sano, M.B., Davalos, R.D., *Biomed. Microdev.*, 2009, 11, 997-1006.

[95] Lewpiriyawong, N., Yang, C., Lam, Y.C., *Microfluid. Nanofluid.*, 2012, 723-33.

[96] Kumar, A., Kwon, J.S., Williams, S.J., Green, N.G., Yip, N.K., Wereley, S.T., *Langmuir*, 2010, 26, 5262-72.

[97] Zhang, Y., Lei, H., Li, Y., Li, B., *Lab Chip*, 2012, 12, 1302-8.

[98] Shi, J., Mao, X., Ahmed, D., Colletti, A., Huang, T.J., *Lab Chip*, 2008, 8, 221-3.

[99] Hammarstrom, B., Evander, M., Barbeau, H., Bruzelius, M., Larsson, J., Laurell, T., Nilsson, J., *Lab Chip*, 2010, 10, 2251-7.

[100] Duhr, S., Braun, D., *Appl. Phys. Lett.*, 2005, 86, 131921.

[101] Afshar, R., Moser, Y., Lehnert, T., Gijs, M.A.M., *Sens. Actuat. B.*, 2011, 154, 73-80.

[102] Bronzeau, S., Pamme, N., *Analytica Chim. Acta.*, 2008, 609, 105-12.

[103] Ramadan, Q., Gijs, M.A.M., Microfluid. Nanofluid., 2012, 13, 529-42.

[104] Fateen, S.K., MIT, PhD dissertation, 2002.

[105] Winkleman, A., Gudiksen, K.L., Ryan, D., Whitesides, G.M., *Appl. Phys. Lett.*, 2004, 85, 2411-3.

[106] Halverson, D., Kalghatgi, S., Yellen, B., Friedman, G., *J. Appl. Phys.*, 2006, 99, 08P504.

[107] Erb, R.M., Yellen, B.B., *J. Appl. Phys.*, 2008, 103, 07A312.

[108] Rosensweig, R.E., *Adv. Electronics electron Phys.*, 1979, 48, 103-99.

[109] Cetin, B., Li, D., *Electrophoresis*, 2011, 32, 2410-27.

[110] Laurell, T., Petersson, F., Nilsson, A., *Chem. Soc. Rev.*, 2007, 36, 492-506.

[111] Lin, S.C., Mao, X., Huang, T.J., *Lab Chip*, 2012, 12, 2766-70.

[112] Cho, S.H., Godin, J.M., Chen, C., Qiao, W., Lee, H., Lo, Y., *Biomicrofluidics*, 2010, 4, 043001.

[113] Kayani, A.A., Khoshmanesh, K., Ward, S.A., Mitchell, A., Kalantar-zadeh, K., *Biomicrofluidics*, 2012, 4, 031501.

[114] Lenshof, A., Laurell, T., *Chem. Soc. Rev.*, 2010, 39, 1203-17.

[115] Bhagat, A.A.S., Bow, H., Hou, H., Tan, S., Han, J., Lim, S., *Med. Biol. Eng. Comput.*, 2010, 48, 999-1014.

[116] Gossett, D.R., Weaver, W.M., Mach, A.J., Hur, S.C., Tse, H.T., Lee, W., Amini, H., Carlo, D.D., *Anal. Bioanal. Chem.*, 2010, 297, 3249-67.

APPENDIX A

DEVICE FABRICATION

The microchannels involved in these projects were made using standard soft lithography. To create the microchannel master, photoresist (SU-8, MicroChem Corp., Newton, MA) was dispensed on an acetone treated glass slide and spun (WS-400E-NPP-Lite, Laurell Technologies, North Wales, PA) at a terminal speed of 800 rpm. Then, the slide was hot plated (HP30A, Torrey Pines Scientific, San Marcos, CA) at 65 °C for 5 minutes and 95°C for 15 minutes as part of the process of a soft bake. Note, for microchannels of differing depth, as seen in chapter 4, this spin coat process is varied with respect to the final terminal speed. Following that, a photomask (designed using AutoCAD® and printed on a transparent film) was placed on top of the slide and the photoresist film underwent UV exposure (ABM Inc., San Jose, CA) at a prescribed dose. Next, a post exposure baking of the slide occurred at 65 °C for 1 minute and 95°C for 4 minutes. Once baking was complete, the photoresist was immersed in SU-8 developer solution for 6 minutes (again, differing for varied channel depth). Finally, the photoresist was rinsed using isopropyl alcohol and allowed to dry at room temperature. The processed photoresist leaves a positive indentation of the microchannel geometry and is ready to be used for channel fabrication.

Once magnets and other objects were in place, liquid PDMS was dispensed to the dish and underwent degassing in an isotemp vacuum oven (13-262-280A, Fisher Scientific, Fair Lawn, NJ) for 30 minutes. Afterwards, the dish was moved into a gravity

convection oven (13-246-506GA, Fisher Scientific, Fair Lawn, NJ) for curing at 65 °C for 3 hours. Following that, the PDMS was cut out and punched with two through holes at designed reservoir locations. Finally the PDMS slab was bonded to a glass slide after plasma treating (PDC-32G, Harrick Scientific, Ossining, NY) for 1 minute.